nature genetics

Article

https://doi.org/10.1038/s41588-023-01339-5

Thymidine nucleotide metabolism controls human telomere length

Received: 12 July 2022

Accepted: 21 February 2023

Published online: 23 March 2023

Check for updates

William Mannherz [1,2,3] & Suneet Agarwal [1,2,3]

Telomere length in humans is associated with lifespan and severe diseases, yet the genetic determinants of telomere length remain incompletely defined. Here we performed genome-wide CRISPR–Cas9 functional telomere length screening and identified thymidine (dT) nucleotide metabolism as a limiting factor in human telomere maintenance. Targeted genetic disruption using CRISPR–Cas9 revealed multiple telomere length control points across the thymidine nucleotide metabolism pathway: decreasing dT nucleotide salvage via deletion of the gene encoding nuclear thymidine kinase (*TK1*) or de novo production by knockout of the thymidylate synthase gene (*TYMS*) decreased telomere length, whereas inactivation of the deoxynucleoside triphosphohydrolase-encoding gene *SAMHD1* lengthened telomeres. Remarkably, supplementation with dT alone drove robust telomere elongation by telomerase in cells, and thymidine triphosphate stimulated telomerase activity in a substrate-independent manner in vitro. In induced pluripotent stem cells derived from patients with genetic telomere biology disorders, dT supplementation or inhibition of *SAMHD1* promoted telomere restoration. Our results demonstrate a critical role of thymidine metabolism in controlling human telomerase and telomere length, which may be therapeutically actionable in patients with fatal degenerative diseases.

Telomeres are repetitive DNA elements flanking linear chromosomes that promote genomic stability[1,2]. Telomere length decreases as cells divide because DNA polymerases cannot fully replicate linear chromosomes[3,4]. When critically short, telomeres initiate cellular senescence, arresting cell division[5]. This shortening is counteracted by telomerase, a reverse transcriptase[6] that uses an RNA template[7], telomerase RNA component (*TERC*), to synthesize new telomeric repeats[8]. In Mendelian randomization studies, long telomeres are associated with increased lifespan[9], while inherited mutations in genes regulating telomere maintenance are associated with lethal diseases manifesting with pulmonary fibrosis, liver cirrhosis and bone marrow failure, collectively termed telomere biology disorders (TBDs)[10–12]. Despite the importance of telomere length homeostasis for cellular function and health, determinants of human telomere length control are incompletely defined[9].

Deoxynucleotide triphosphates (dNTPs) are common precursors for genome replication by DNA polymerases and telomere elongation by telomerase. Disruptions to DNA precursor metabolism can impair genome replication and are associated with genome instability, mitochondrial genetic diseases and cancer[13–17]. Telomere synthesis occurs via a unique reverse transcription mechanism involving the ratcheting of an RNA template to generate hexanucleotide (5′-GGTTAG-3′) repeats, with distinct dynamics and substrate preferences compared with DNA polymerases[18]. Despite evidence that nucleotide levels influence the enzymatic activity of reconstituted telomerase[19–24], a role for dNTP metabolism in regulating telomere length in humans at a cellular or organismal level has not been directly established. In this article, we take advantage of methodologic advances[25,26] to perform a genome-wide functional screen for human telomere length regulators.

[1]Division of Hematology/Oncology and Stem Cell Program, Boston Children's Hospital, Boston, MA, USA. [2]Pediatric Oncology, Dana-Farber Cancer Institute, Boston, MA, USA. [3]Biological and Biomedical Sciences Program, Harvard/MIT MD-PhD Program, Harvard Stem Cell Institute, Harvard Initiative for RNA Medicine, and Department of Pediatrics, Harvard Medical School, Boston, MA, USA. e-mail: suneet.agarwal@childrens.harvard.edu

https://doi.org/10.1038/s41588-023-01339-5

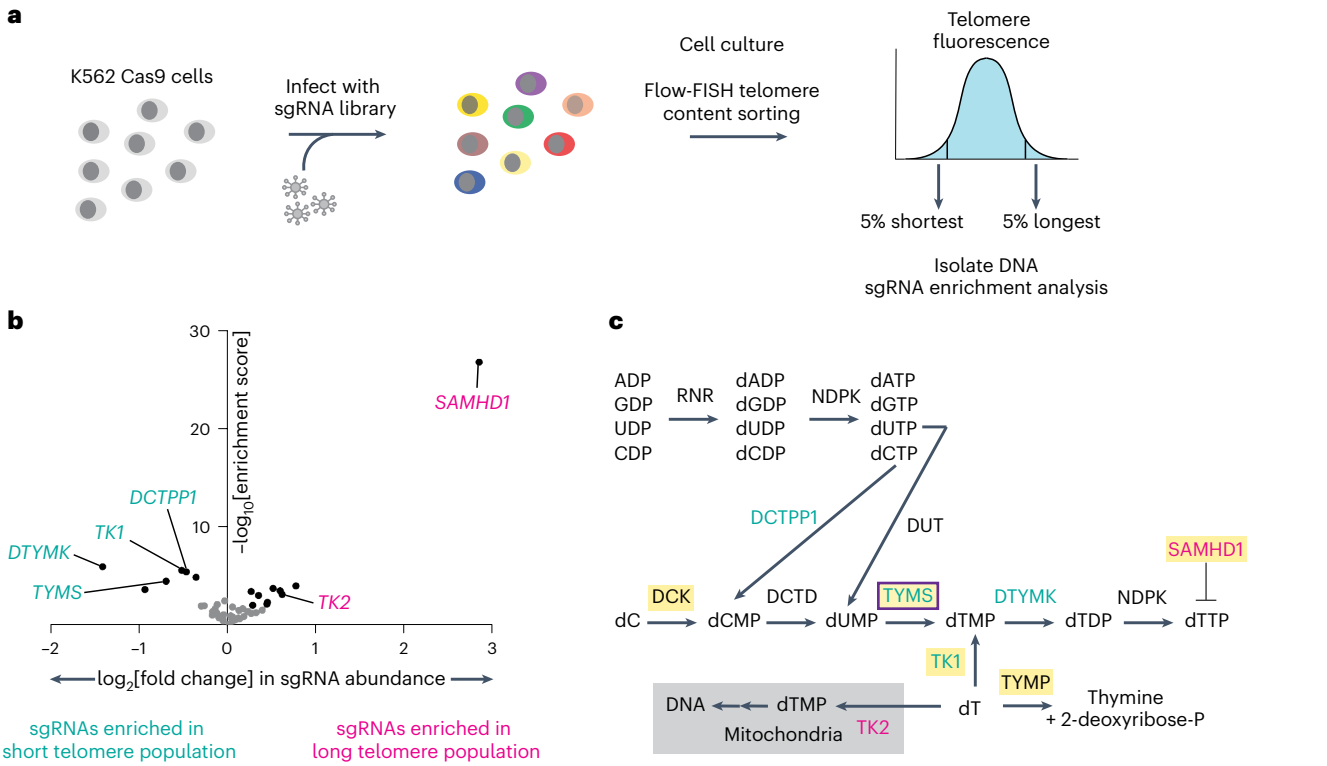

Fig. 1 | Telomere length CRISPR–Cas9 screening reveals that dT nucleotide metabolism genes are required for telomere length control. a, Diagram of the flow-FISH telomere content-screening strategy. Cas9-expressing K562 cells are transduced with an sgRNA library, cultured for weeks at split ratios sufficient to maintain library representation and sorted by flow-FISH to isolate cells with the highest and lowest 5% of telomere fluorescence. **b**, Results of CRISPR–Cas9 screening, performed in duplicate, of 53 nucleotide metabolism genes with ten sgRNAs per gene and 200 nontargeting control sgRNAs. sgRNA enrichment was analyzed using the MAGeCK RRA. The RRA gene enrichment score is plotted against the $\log_2$[fold change] of sgRNA abundance in high versus low fifth percentile TelC-A647 fluorescence populations. The black dots represent genes significantly enriched in long or short populations with a false discovery rate of <0.05, as calculated via the Benjamini–Hochberg procedure. sgRNAs targeting genes labeled in blue and pink were enriched in the in the short and long telomere populations, respectively. **c**, Diagram of dT nucleotide metabolism. Products of genes identified in recent telomere length GWASs[9,34] are highlighted. The gene encoding TYMS (boxed) was recently associated with dyskeratosis congenita[35]. ADP, adenosine diphosphate; CDP, cytidine diphosphate; dADP, deoxyadenosine diphosphate; dATP, deoxyadenosine triphosphate; dC, deoxycytidine; dCDP, deoxycytidine diphosphate; dCMP, deoxycytidine monophosphate; dCTP, deoxycytidine triphosphate; dGDP, deoxyguanosine diphosphate; dGTP, deoxyguanosine triphosphate; dTDP, thymidine diphosphate; dUDP, deoxyuridine diphosphate; dUTP, deoxyuridine triphosphate; GDP, guanosine diphosphate; NDPK, nucleoside diphosphate kinase; RNR, ribonucleotide reductase; UDP, uridine diphosphate.

We identify thymidine (dT) nucleotide metabolism as a critical regulator of human telomere length, advancing our understanding of cellular metabolic pathways required for genomic integrity and pointing to potential novel therapies for lethal diseases with high unmet need.

Results

CRISPR screening links thymidine flux and telomere length

Fluorescence in situ hybridization using a peptide nucleic acid (PNA) telomere repeat probe coupled with flow cytometry (flow-FISH) is a clinically validated telomere length assay performed on single cells[26,27]. We used flow-FISH as a phenotypic readout for CRISPR–Cas9 screening in human cells to identify novel genes regulating telomere length (Fig. 1a). K562 cells expressing SpCas9 (Extended Data Fig. 1a–c) were transduced with the Brunello genome-wide guide RNA (sgRNA) library[25] and cultured for 49 d, followed by isolation of cells harboring the longest and shortest fifth percentiles of telomere length using flow-FISH (Extended Data Fig. 1d–g). We isolated gDNA from the sorted populations, performed deep sequencing and analyzed sgRNA representation using the MAGeCK robust rank algorithm (RRA)[28] (Extended Data Fig. 1h,i). We found that sgRNAs targeting telomerase reverse transcriptase (*TERT*) were enriched in the short telomere population, while sgRNAs targeting several components of shelterin—a telomere chromatin protein complex that negatively regulates telomere length[29–32]—were enriched in the long telomere population, including *POT1*, *TERF1* and *TERF2IP* (*RAP1*). These data validate our CRISPR screening strategy to identify tolerable genetic loss of function associated with human telomere length.

Unbiased pathway analysis of screening hits using MAGeCKFlute[33] revealed that sgRNAs targeting pyrimidine nucleotide metabolism genes were enriched in the cell population with short telomeres (Extended Data Fig. 1j). Recent genome-wide association studies (GWASs) have also implicated nucleotide metabolism genes in telomere length control[9,34], and mutations at the thymidylate synthase (*TYMS*) locus have been newly identified in patients presenting with the TBD dyskeratosis congenita[35]. Based on our screening results and the emerging human genetic data, we performed a second round of screening using a custom sgRNA library targeting 53 nucleotide metabolism genes. Comparing sgRNAs enriched in the sorted long and short telomere populations, we identified several genes implicated specifically in thymidine nucleotide metabolism (Fig. 1b,c). In cells with short telomeres, we saw enrichment of sgRNAs targeting genes predicted to promote dT nucleotide synthesis, including *DTYMK*, *TYMS*, *TK1* (ref. [36]) and *DCTPP1* (ref. [37]). Conversely, sgRNAs targeting genes predicted to reduce nuclear dT nucleotide levels,

https://doi.org/10.1038/s41588-023-01339-5

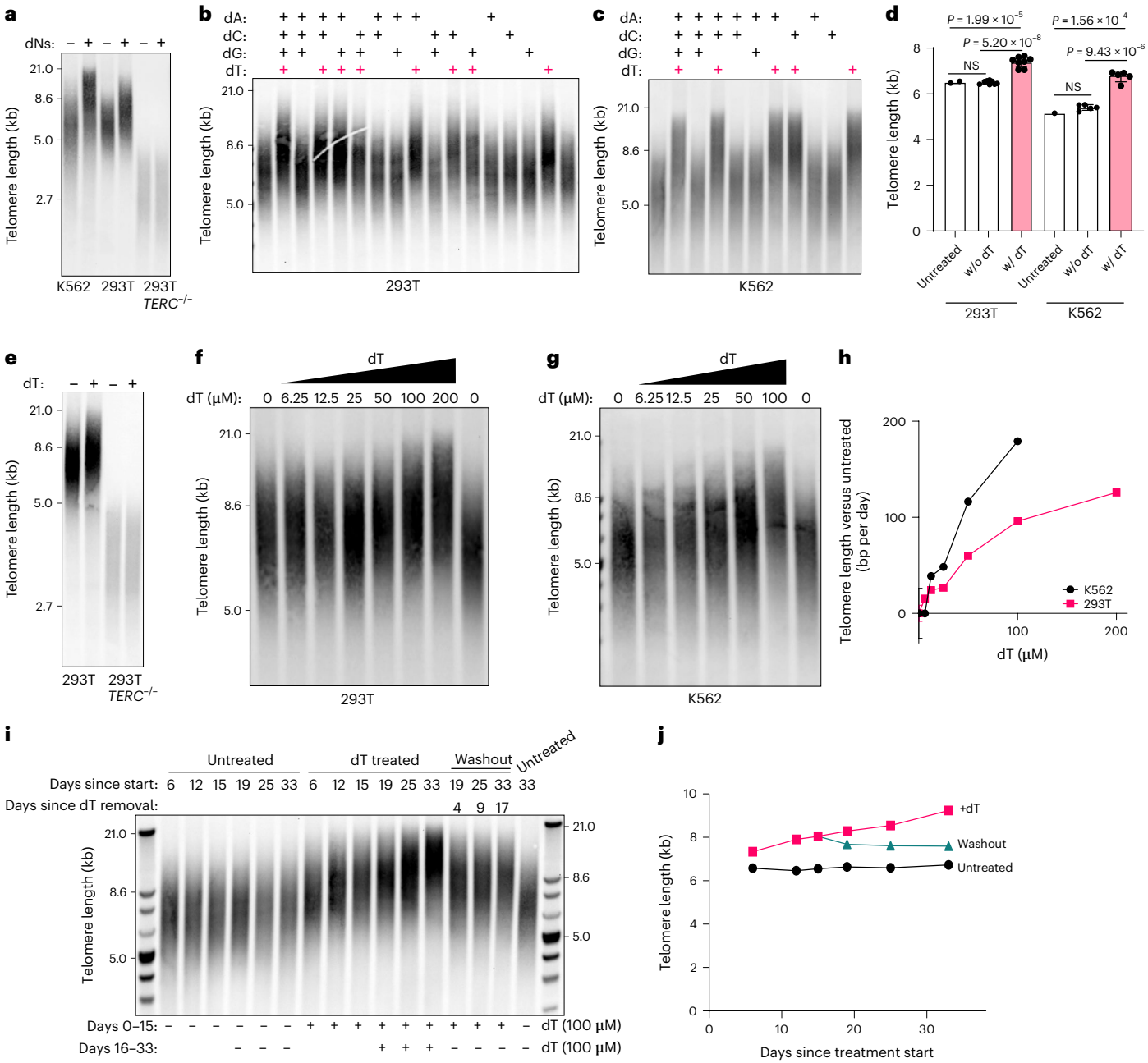

Fig. 2 | dT treatment drives telomerase-dependent telomere lengthening in human cells. a, TRF Southern blot probed for the telomere repeat of K562, 293T or *TERC*-null (*TERC*$^{-/-}$) 293T cells treated with or without dNs (100 μM each of dA, dC, dG and dT) for 8 d. **b**, TRF of 293T cells treated with 100 μM of the indicated dNs for 9 d. Untreated lanes are technical replicates. **c**, TRF of K562 cells treated with 100 μM of the indicated dNs for 8 d. **d**, Quantification of **b** and **c** (see Methods). Numbers of samples were as follows: $n = 8$ for 293T cells with or without dT and $n = 5$ for K562 cells with or without dT. Statistical significance was determined by one-way analysis of variance (ANOVA) with Bonferroni correction for multiple comparisons for each cell line. The data are presented as means ± s.d. NS, not significant ($P > 0.05$). **e**, TRF of 293T or 293T *TERC*$^{-/-}$ cells treated with or without 100 μM dT for 7 d. **f**, TRF of 293T cells treated with the indicated dose of dT for 10 d. **g**, TRF of K562 cells treated with the indicated dose of dT for 8 d. **h**, Quantification of **f** and **g**, as in **d**. **i**, 293T cells treated with or without 100 μM dT for the indicated period of time. On day 15, dT-treated cells were split and continued to be cultured either with or without 100 μM dT for the indicated number of days. Day 33 untreated lanes are technical replicates. **j**, Quantification of **i**. The results presented in this figure represent single experiments.

including the deoxynucleoside triphosphohydrolase (dNTPase) *SAMHD1* (refs. [38–40]), were enriched in cells with long telomeres. Taken together, these results point to dT nucleotide levels as a novel regulator of telomere length in human cells.

dT treatment increases telomere length in human cells

Based on these data, we tested whether manipulation of nucleotides could alter telomere length in human cells. Deoxyribonucleoside (dN) supplementation can increase cellular nucleotide levels via salvage pathway kinases[36,41]. Remarkably, supplementing K562 or 293T cell culture media with the four canonical dNs drove rapid telomere lengthening by thousands of nucleotides within 8 d (Fig. 2a). When we repeated the experiment in telomerase-negative *TERC*-null 293T cells (Fig. 2a and Extended Data Fig. 2a–g), we found no increase in telomere length, indicating that telomerase is required for dN-mediated telomere lengthening. To identify which dNs promote telomere elongation,

we treated 293T (Fig. 2b) and K562 cells (Fig. 2c) with dNs individually or in combination. We found that all combinations that included dT promoted telomere lengthening, as did dT alone, while no combination lacking dT elongated telomeres (Fig. 2b–d). Again, dT treatment of telomerase-negative *TERC*-null 293T cells failed to drive detectable telomere elongation (Fig. 2e). Collectively, these results demonstrate that dT supplementation alone can drive rapid and robust telomere elongation in human cells in a telomerase-dependent manner, and offer an explanation for the genetic data implicating nucleotide biosynthetic pathways in human telomere length regulation.

Next, we evaluated how treatment with escalating doses of dT impacted telomere length. We found a continuous dose response in telomere elongation after dT treatment up to 200 µM in 293T cells and 100 µM in K562 cells (Fig. 2f–h). We confirmed that dT from different manufacturers, each of >98% purity, promoted telomere elongation similarly (Extended Data Fig. 3a). To study the kinetics of telomere length changes after dT treatment and its withdrawal, we performed a time course analysis in 293T cells and found that dT supplementation gradually and continually increased telomere length over 33 d (Fig. 2i,j). Withdrawal of dT after 15 d aborted telomere elongation, indicating that the effects of dT on telomere length depend on exposure rather than triggering autonomous telomere lengthening mechanisms (Fig. 2i,j). These data indicate that dT supplementation promotes gradual, exposure-dependent and reversible telomere elongation in human cells.

TK1 is required for telomere lengthening by dT

dT salvage occurs through distinct pathways to generate thymidine triphosphate (dTTP) for mitochondrial versus nuclear genome synthesis (Fig. 3a). Thymidine kinase 1 (TK1) acts in the cytosol to generate deoxythymidine monophosphate (dTMP) available for nuclear genome replication, while thymidine kinase 2 (TK2) acts in mitochondria to generate dT nucleotides for mitochondrial genome synthesis[13]. As telomeres reside in the nuclear genome, we hypothesized that dT-mediated telomere lengthening requires functional TK1 but not TK2. To test this hypothesis, we electroporated 293T or K562 cells with SpCas9 and sgRNAs targeting either *TK1* or *TK2*, or with an sgRNA targeting the *AAVS1* control locus (Extended Data Fig. 3b,c). Consistent with our hypothesis, we found that *TK1*-edited cells showed a complete abrogation of telomere lengthening after dT treatment (Fig. 3b–e), whereas *TK2*-edited cells showed telomere length increases equivalent to control *AAVS1*-targeted cells (Fig. 3b–e) in the presence of dT. Without dT treatment, we found modest telomere length decreases in *TK1* knockout cells (Fig. 3b,d and Extended Data Fig. 3d), as anticipated from our screening data. These results indicate that cytosolic phosphorylation of dT to generate dTMP by TK1 is required for telomere lengthening after dT treatment. To assess how dT supplementation alters cellular nucleotide levels, we performed liquid chromatography–mass spectrometry[42] on 293T cells treated with 100 µM dT for 24 h and found that dT treatment increased levels of dTMP, thymidine diphosphate (dTDP) and dTTP (Extended Data Fig. 3e). These data are consistent with our genetic data showing that dT exerts its effects on telomere length by conversion into dT nucleotides.

TYMS is required for telomere lengthening by deoxyuridine

As an alternative to dT salvage, dTMP can be de novo synthesized from deoxyuridine monophosphate (dUMP) by TYMS using one carbon transfer from 5,10-methylene-tetrahydrofolate (Fig. 3f). Deoxyuridine (dU) nucleoside can be salvaged via TK1 to form dUMP[36]. Therefore, we tested the impact of dU supplementation in 293T cells and found telomere elongation to a degree similar to dT over the course of 10 d, albeit at 10× the concentration (1 mM) (Extended Data Fig. 3f). Folate, however, did not appear to be limiting as its supplementation in 293T cells did not yield telomere elongation (Extended Data Fig. 3f). To test whether dU increases telomere length via conversion of dUMP to dTMP by TYMS (Fig. 3f), we targeted *TYMS* in 293T and K562 cells using CRISPR–Cas9 (Extended Data Fig. 3g). *TYMS*-deficient cells required salvaged dT for survival; thus, both *TYMS*-edited and control *AAVS1*-edited cells were treated with a baseline level of 16 µM dT. We then treated cells with either 100 µM additional dT (116 µM total) or 1 mM dU for 10 d and evaluated telomere length. We found that *TYMS*-knockout cells remained responsive to increased doses of dT to promote telomere lengthening, while dU could no longer promote telomere lengthening in *TYMS*-deficient cells (Fig. 3g–j). Collectively, these results show that dU lengthens telomeres via conversion into dTMP, and that in cells with deficient de novo dT nucleotide synthesis machinery due to *TYMS* inactivation, dT supplementation can increase dT nucleotide levels via the salvage pathway to lengthen telomeres.

SAMHD1 restricts human telomere length

Sterile alpha motif and HD domain-containing protein 1 (SAMHD1) regulates cellular dNTP levels by degrading all four canonical dNTPs, including dTTP, into dNs[38–40] (Fig. 4a). This function has been suggested to restrict retroviruses by limiting dNTP pools available for reverse transcription[38,43]. In our screen for telomere length regulators, *SAMHD1* sgRNAs drove robust telomere elongation (Fig. 1b). Recent biochemical studies have shown that SAMHD1 is enriched at telomeric chromatin[44], and GWASs have associated *SAMHD1* with human telomere length[9]. However, effects of manipulating SAMHD1 on human telomere length have not been shown. We therefore directly evaluated how disruption of *SAMHD1* could impact telomere length homeostasis in human cell lines. We found that deletion of *SAMHD1* by CRISPR–Cas9 was tolerated and lengthened telomeres by thousands of nucleotides in 27 d (Fig. 4b and Extended Data Fig. 4a), in line with our screening results. Inhibiting SAMHD1 using short hairpin RNA (shRNA)-mediated RNA interference also showed a telomere lengthening effect (Fig. 4c,d and Extended Data Fig. 4b–e). In *TERC*-null 293T cells, however, we found no change in telomere length upon *SAMHD1* knockout or knockdown (Fig. 4e,f and Extended Data Fig. 4e), indicating that telomere lengthening due to SAMHD1 loss of function occurs by a telomerase-dependent mechanism. These results show that SAMHD1 controls telomere length in human cells.

Because SAMHD1 is known to degrade dTTP[38,40] (Fig. 4a), we asked whether SAMHD1 restricts the degree of telomere lengthening from dT treatment. At 5 d after transduction with a *SAMHD1*-targeting shRNA, we treated cells with or without 50 µM dT for 8 d. We found that the combined effect of *SAMHD1* knockdown and dT treatment produced greater telomere lengthening (823 ± 33 base pairs (bp)) compared with dT treatment alone (514 ± 63 bp) (Fig. 4g,h). SAMHD1 has several proposed functions beyond its dNTPase activity, including contributing to homology-directed repair and replication fork progression[45,46]. To investigate whether SAMHD1 dNTPase activity restricts dT-mediated telomere lengthening, we overexpressed two different dNTPase-deficient versions of SAMHD1 in cells[47,48]. We found that overexpression of wild-type SAMHD1 decreased telomere lengthening following dT treatment, compared with control cells overexpressing enhanced green fluorescent protein (eGFP). In contrast, overexpression of dNTPase-deficient SAMHD1 variants (with either substitution of His with Ala at amino acid residue 215 or substitution of Lys with Ala at amino acid residue 312) could not restrict telomere lengthening from dT to the same degree (Fig. 4i–l and Extended Data Fig. 4f). Collectively, these data indicate that SAMHD1 dNTPase activity regulates telomere length homeostasis in human cells, and point to dTTP as a downstream metabolite promoting telomere elongation after dT supplementation.

dT elongates telomeres without inhibiting cell growth

dT is commonly used to inhibit cell cycle progression, arresting cells in the S phase at doses in the millimolar range[49,50]. We asked whether dT-mediated telomere lengthening could be dissociated from cell cycle effects of dT. When 293T cells were treated with increasing doses of

https://doi.org/10.1038/s41588-023-01339-5

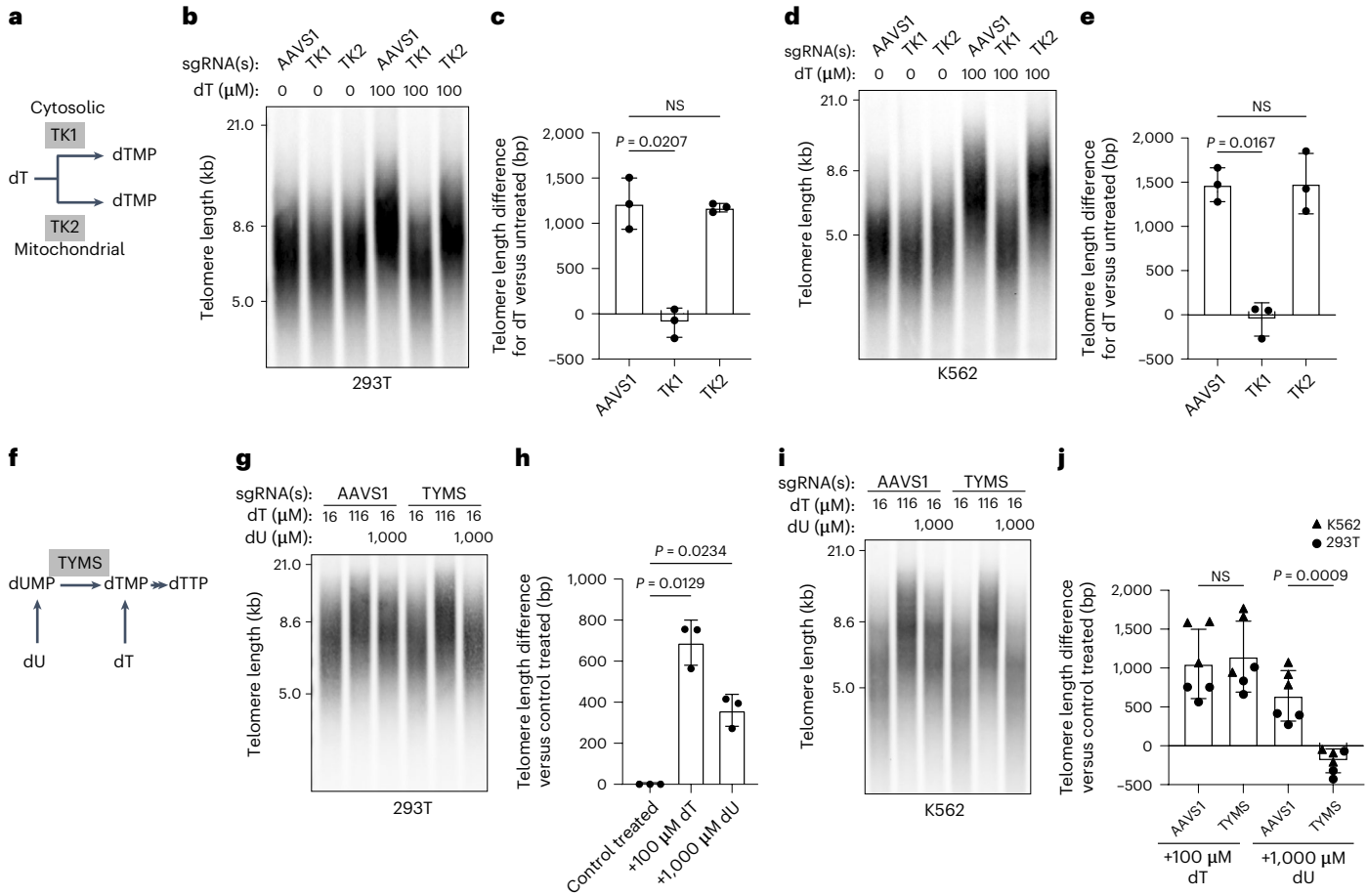

Fig. 3 | dT nucleotide metabolism genes control dT-mediated telomere lengthening. a, Diagram of dT salvage. **b**, Representative TRF of 293T cells targeted with Cas9 and the indicated sgRNA, followed by treatment with the indicated dose of dT for 14 d. **c**, Quantification of **b** ($n = 3$ biological replicates). Statistical significance was determined by one-way repeated measures ANOVA with Geisser–Greenhouse correction and Dunnett's multiple comparison test. **d**, Representative TRF of K562 cells targeted with Cas9 and the indicated sgRNA, followed by treatment with the indicated dose of dT for 10 d. **e**, Quantification of **d**, as in **c** ($n = 3$ biological replicates). **f**, Diagram of dT and dU salvage. **g**, Representative TRF of 293T cells targeted with Cas9 and the indicated sgRNA, followed by treatment with the indicated doses of dT and dU for 10 d. **h**, Quantification of the median telomere lengths shown in **g**, as in **c** ($n = 3$ biological replicates). **i**, Representative TRF of K562 cells targeted with Cas9 and the indicated sgRNA, followed by treatment with the indicated doses of dT and dU for 10 d. **j**, Quantification of the median telomere lengths shown in **g** and **i**. Statistical significance was determined by one-way repeated measures ANOVA with Geisser–Greenhouse correction and Bonferroni's multiple comparison test ($n = 3$ biological replicates for each cell line). The data in **c**, **e**, **h** and **j** are presented as means ± s.d.

dT, growth was minimally impacted at doses below 100 μM (Fig. 5a). We therefore chose doses with no discernable effects on growth and evaluated their impact on telomere length. We found that supplementation of 293T cells with 20 or 40 μM dT for 34 d drove robust telomere lengthening with undetectable impact on cellular growth (Fig. 5b–d). Similar results were seen in K562 cells treated with low doses of dT for 34 d (Fig. 5e–g). DNA content staining and flow cytometry similarly showed no detectable changes in cell cycle distribution at dT doses below 100 μM in 293T cells and below 12.5 μM in K562 cells (Extended Data Fig. 5a–d). These data indicate that the slowing of cell growth is not required for telomere lengthening from dT treatment.

dT elongates telomeres without replication stress

dT supplementation increases levels of dTTP and can decrease deoxycytidine triphosphate levels, leading to replication stress at high doses. Because replication stress signaling has been implicated in telomerase biology[51–53], we asked whether replication stress induction explained the telomere length increases seen with dT treatment. First, we tested whether telomere elongation is a universal response to replication stress-inducing compounds. When we treated 293T cells with aphidicolin, which inhibits DNA polymerases, at doses maximally tolerated for cell growth, we found telomere elongation after 10 d (Extended Data Fig. 6a), as previously observed[53]. However, treatment with hydroxyurea, which blocks deoxyribonucleotide production by ribonucleotide reductase (Fig. 6a), up to doses permissible for cell growth did not change telomere length after 10 d (Extended Data Fig. 6a). This suggested that replication stress induction may not cause telomere elongation in all cases. However, cytotoxicity limited our ability to apply higher doses of replication stress-inducing compounds for time periods long enough to study telomere length changes. To study the relationship between replication stress, dT and telomere length more acutely, we transfected *TERC*-null 293T cells with expression vectors encoding *TERT* and *TERC*, generating super-telomerase cells[54], which showed telomere elongation within 2 d (Extended Data Fig. 6b, lanes 1 and 3). Remarkably, we found that treatment of super-telomerase cells with dT for only 30 h robustly increased telomere repeat synthesis in a dose-responsive and telomerase-dependent manner (Fig. 6b and Extended Data Fig. 6b (lanes 3 and 4)). Of note, this effect could be observed with only 40 μM dT, far below doses that induce replication stress signaling as measured by immunoblotting for pCHK1-S345 and pRPA32-S33

https://doi.org/10.1038/s41588-023-01339-5

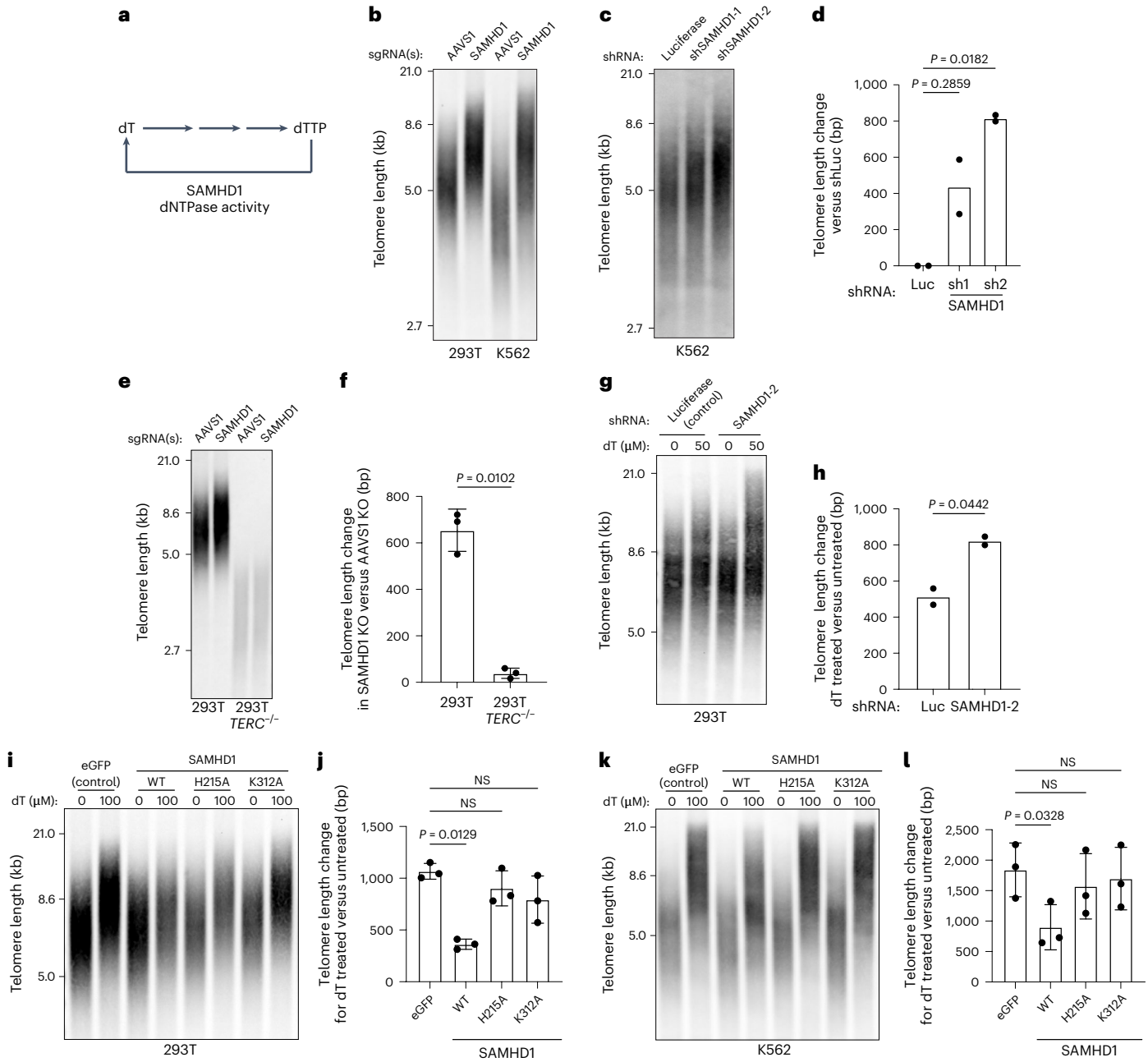

Fig. 4 | SAMHD1 restricts human telomere length and limits dT-mediated telomere elongation. a, Diagram of SAMHD1 dNTPase activity. **b**, TRF of 293T or K562 cells cultured for 27 d following Cas9-sgRNA targeting with the indicated sgRNA. The results represent a single experiment. **c**, Representative TRF of K562 cells cultured for 33 d following infection with an shRNA expression construct targeting luciferase (control) or SAMHD1. **d**, Quantification of the telomere lengths shown in **c**. Statistical significance was determined by one-way repeated measures ANOVA with Geisser–Greenhouse correction and Dunnett's multiple comparison test ($n = 2$ biological replicates). **e**, Representative TRF of 293T or 293T *TERC*$^{-/-}$ cells cultured for 14 d following Cas9-sgRNA targeting with the indicated sgRNA. **f**, Quantification of **e**. Statistical significance was determined by paired two-sided *t*-test ($n = 3$ biological replicates). KO, knockout. **g**, Representative TRF of 293T cells transduced with the indicated shRNA construct, then supplemented with the indicated dose of dT for 8 d. **h**, Quantification of **g**, as in **f** ($n = 2$ biological replicates). **i**, Representative TRF of 293T cells overexpressing eGFP or SAMHD1 of the indicated genotype and supplemented with the indicated dose of dT for 10 d. H215A represents substitution of His with Ala at amino acid residue 215 and K312A represents substitution of Lys with Ala at amino acid residue 312. WT, wild type. **j**, Quantification and statistical analysis of **i**, as in **d** ($n = 3$ biological replicates). **k**, Representative TRF of K562 cells manipulated as in **i**. **l**, Quantification and statistical analysis of **k**, as in **d** ($n = 3$ biological replicates). The data in **d**, **f**, **h**, **j** and **l** are presented as means and error bars indicate s.d.

(Fig. 6c), and below those that substantially impacted cell cycle progression (Fig. 6d and Extended Data Fig. 6e). Using this system, we next asked how high-dose treatment with replication stress-inducing agents such as aphidicolin, hydroxyurea and the TYMS inhibitor 5-fluorouracil (5FU) influence telomere synthesis compared with dT. We found that treatment of super-telomerase cells with aphidicolin for 30 h drove detectable increases in telomere length, albeit to a lesser extent than dT (Fig. 6e). However, rather than elongating telomeres like dT or aphidicolin, treatment with hydroxyurea or 5FU ablated telomere elongation by telomerase (Fig. 6f,g). Despite the markedly different

https://doi.org/10.1038/s41588-023-01339-5

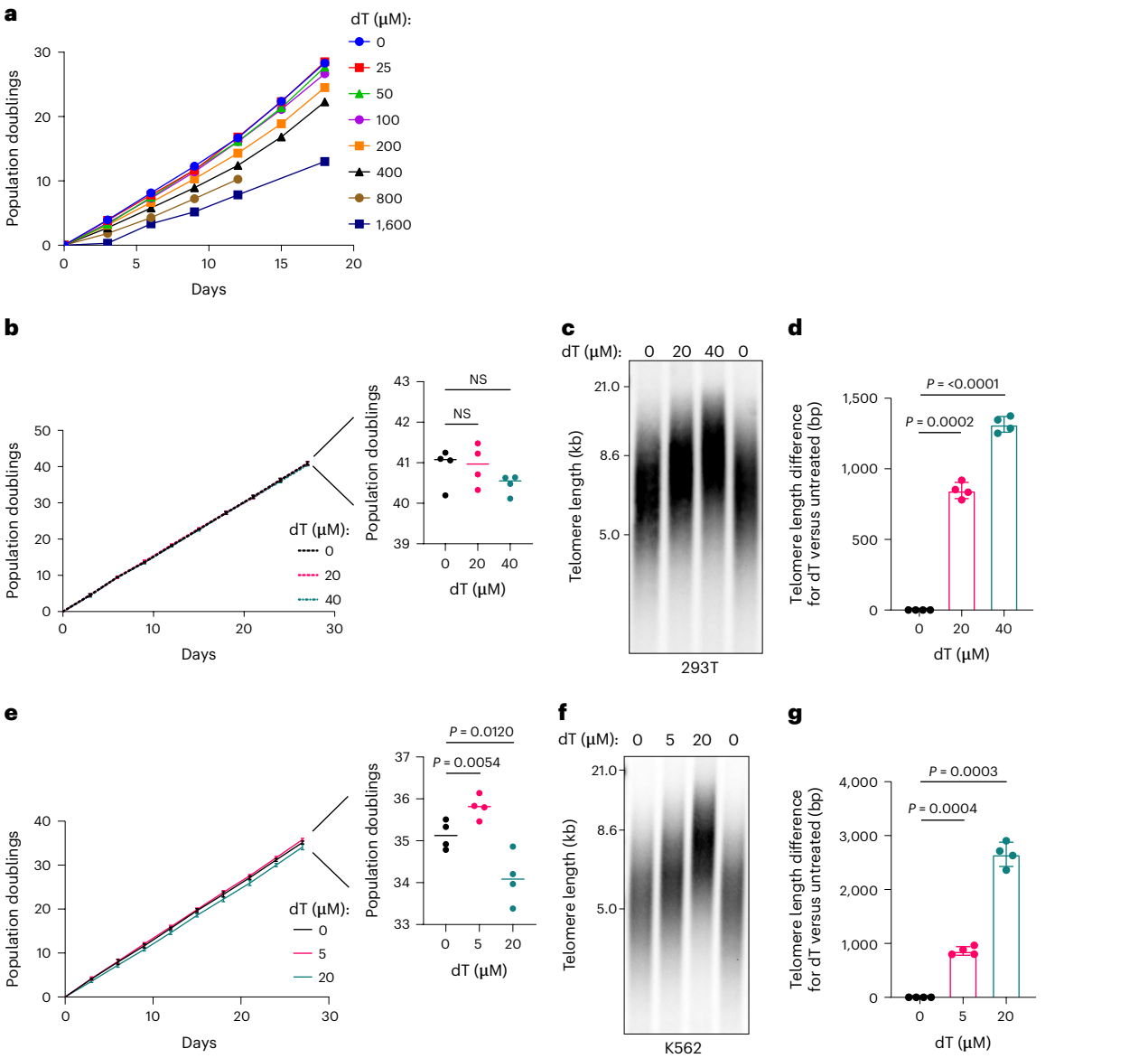

Fig. 5 | Telomere lengthening from dT treatment occurs without inhibiting cell growth. a, Growth curves of 293T cells treated with the indicated doses of dT. **b**, Growth curves of 293T cells treated with the indicated doses of dT ($n = 4$ biological replicates). Inset, graph showing population doublings after 27 d. Statistical significance was determined by one-way repeated measures ANOVA with Geisser–Greenhouse correction and Dunnett's multiple comparison test. **c**, Representative TRF of the 293T cells from **b** after 34 d of culture in media containing the indicated dose of dT. **d**, Quantification of **c** ($n = 4$ biological replicates). Statistical significance was determined as in **b**. **e**, Growth curves of K562 cells treated with the indicated dose of dT ($n = 4$ biological replicates). Inset, graph showing population doublings after 27 d. Quantification and statistical analysis were as in **b**. **f**, Representative TRF of the K562 cells from **e** after 34 d of culture in media containing the indicated dose of dT. **g**, Quantification of **f** ($n = 4$ biological replicates). Statistical significance was determined as in **b**. The data in **b**, **d**, **e** and **g** are presented as means and error bars indicate s.d.

effects on telomere biology seen at the highest doses of dT, aphidicolin, 5FU or hydroxyurea, all induced similar levels of replication stress signaling (Fig. 6h,i) and had similar impacts on cell cycle progression (Fig. 6j–l and Extended Data Fig. 6f–h). Collectively, these data show that replication stress signaling induction does not universally promote telomere synthesis and does not explain the telomere lengthening in cells treated with dT at low doses.

Substrate-independent enhancement of telomerase by dTTP

The time frame and magnitude of the effects of dT and 5FU on telomeres in super-telomerase cells strongly suggested that dT nucleotides might directly impact telomerase activity. Given that high-dose 5FU completely inhibited telomere elongation in super-telomerase cells (Fig. 6g) and acts by inhibiting TYMS to limit de novo dTTP production, we asked whether dT supplementation could rescue telomere synthesis following 5FU treatment. Indeed, we found that dT treatment restored telomere elongation despite maximal doses of 5FU (Fig. 6m). These data show that 5FU inhibits telomerase activity by limiting de novo dT nucleotide production and provide further evidence that dT nucleotide synthesis is required for telomerase activity.

The effects of dT nucleotides on telomerase activity could be from increasing the quantity of telomerase holoenzymes per cell, or alternatively by enhancing telomerase function. To test the former possibility, we measured the abundance of active telomerase enzymes in cells using the telomeric repeat amplification protocol (TRAP) assay and found no difference in telomerase activity in lysates from 293T cells treated

https://doi.org/10.1038/s41588-023-01339-5

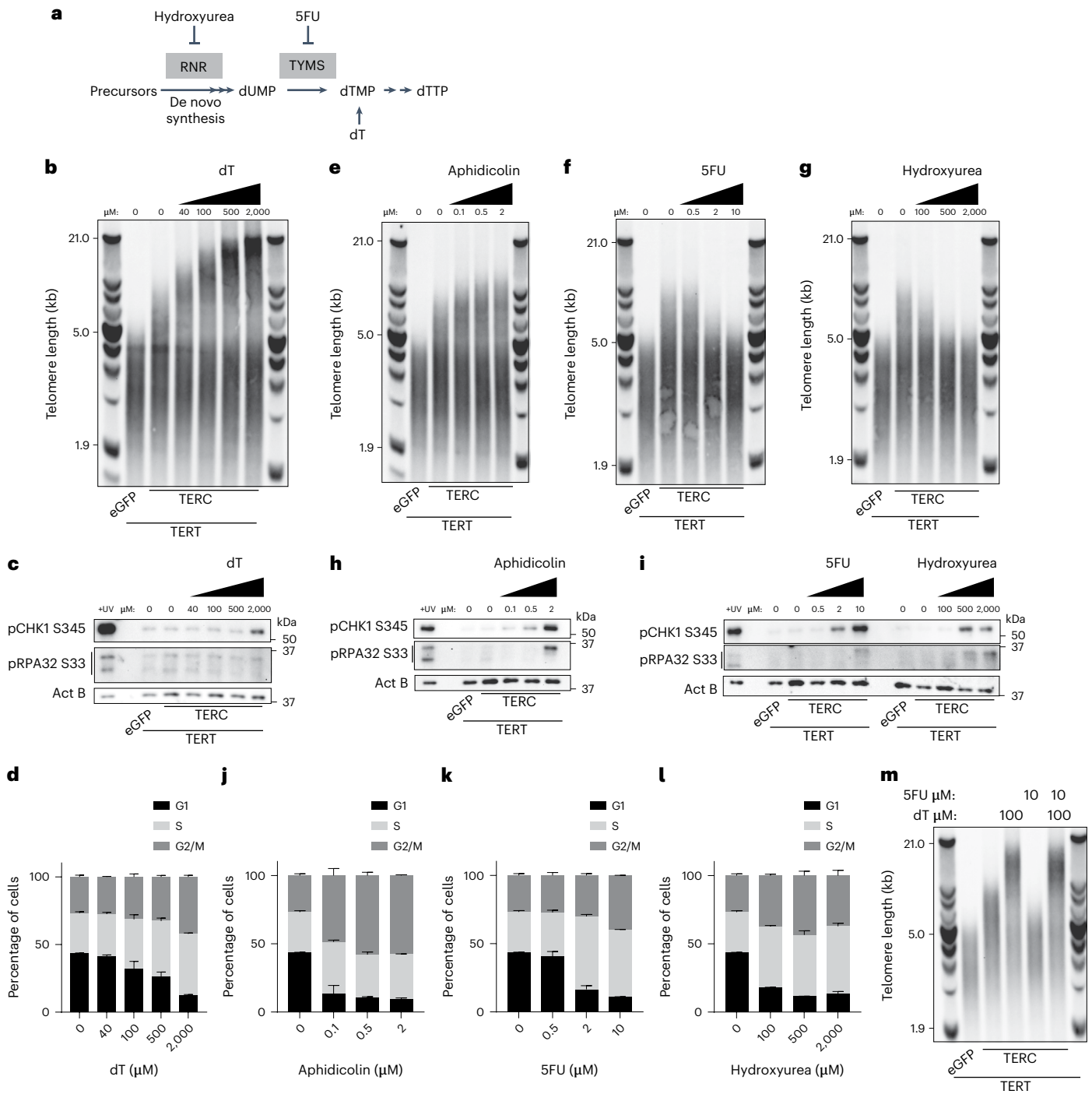

Fig. 6 | Induction of replication stress is insufficient to explain telomere lengthening from dT treatment. a, Diagram of the effect of dT, 5FU and hydroxyurea on dT nucleotide metabolism. **b**, TRF Southern blot of 293T *TERC*$^{-/-}$ cells transfected with the indicated expression vectors, cultured for 18 h and then treated with the indicated dose of dT for 30 h. A representative blot is shown from two biological replicates. **c**, Immunoblot of the cells from **b** using the indicated primary antibodies. Ultraviolet-treated (+UV) 293T cells were used as a positive control. **d**, Cell cycle analysis of the cells from **b**, as measured by DAPI staining and flow cytometry, displaying the percentage of cells in each gate. Data from four biological replicates for untreated cells and from two biological replicates for treated cells are shown. The error bars indicate s.d. **e**–**g**, TRF Southern blots of 293T *TERC*$^{-/-}$ cells transfected with the indicated expression vectors, cultured for 18 h and then treated with the indicated doses of aphidicolin (**e**), 5FU (**f**) or hydroxyurea (**g**) for 30 h. One representative blot is shown for each, from two biological replicates. **h,i**, Immunoblots of the cells from **e** (**h**) and **f** and **g** (**i**), as in **c**. **j**–**l**, Cell cycle analysis of the cells in **e**–**g**, respectively, by DAPI staining and flow cytometry, as in **d**. Data from four biological replicates for untreated cells and from two biological replicates for treated cells are shown. Untreated samples were the same as in **d**. **m**, TRF Southern blot of 293T *TERC*$^{-/-}$ cells transfected with the indicated expression vectors, cultured for 18 h and then treated with the indicated doses of 5FU and dT for 30 h. The data in **d**, **j**, **k** and **l** are presented as means and error bars indicate s.d. Full-length western blots are provided as source data.

with or without 100 μM dT (Fig. 7a,b). These data indicate that dT treatment does not change the overall quantity of telomerase holoenzymes in cells. Next, to test the effects of dTTP on telomerase function in vitro, we performed the TRAP assay with increasing levels of exogenous dTTP and found enhanced telomerase activity (Extended Data Fig. 7a,b). However, because dTTP is a direct substrate for GGTTAG

https://doi.org/10.1038/s41588-023-01339-5

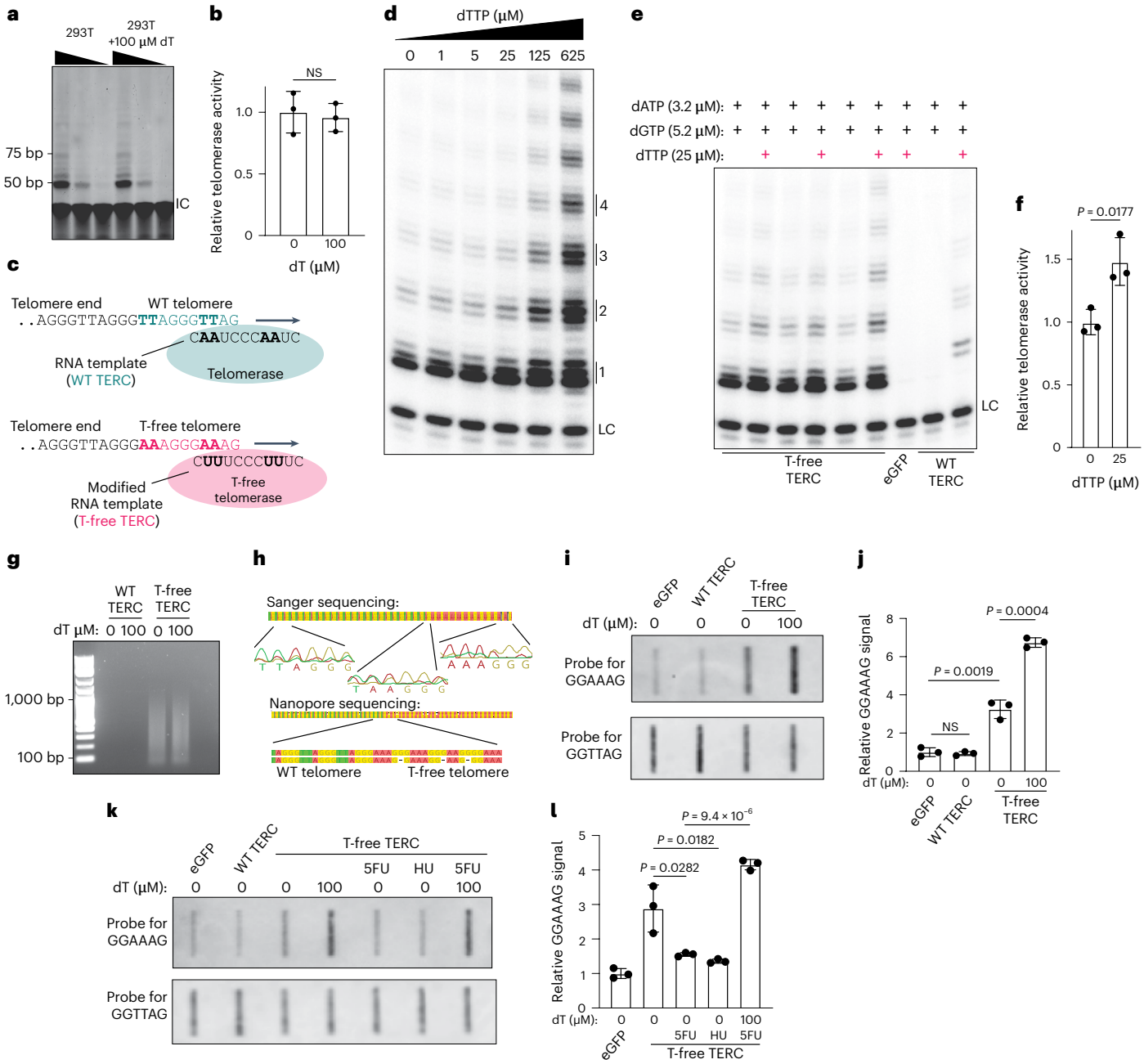

Fig. 7 | dT nucleotides enhance human telomerase activity independent of dTTP's role as a telomerase substrate. a, Representative TRAP assay of 293T cells treated as indicated for 3 d. IC, internal control product. **b**, Quantification of **a** ($n = 3$ biological replicates). Statistical significance was determined by unpaired two-sided *t*-test. **c**, Diagram of wild-type and T-free telomerase. **d**, Direct telomerase assay using immunopurification of overexpressed, tagged TERT cotransfected with T-free TERC into 293T *TERC*$^{-/-}$ cells. LC, loading control (a 16-nucleotide ^{32}P-end-labeled oligo). Telomerase repeat products are numbered. **e**, Direct telomerase assay using immunopurification of overexpressed, tagged TERT cotransfected with the indicated *TERC* vector or *eGFP* as a control into 293T *TERC*$^{-/-}$ cells ($n = 3$ replicates). **f**, Quantification of **e**. Statistical significance was determined as in **b**. **g**, PCR to detect wild-type and T-free telomere junctions (see Methods), performed on 293T *TERC*$^{-/-}$ cells transfected with the indicated vectors, cultured for 18 h and then treated with dT as indicated for 3 d. **h**, Sanger and nanopore sequencing of the products from lane 4 in **g**. The Sanger trace corresponding to cytosine has been omitted for clarity. **i**, Slot blot of DNA from 293T *TERC*$^{-/-}$ cells overexpressing TERT as well as the indicated vector, cultured for 18 h and then treated with the indicated dose of dT for 30 h, performed in technical triplicates. Representative data from one of two biological replicates are displayed. **j**, Quantification of GGAAAG signal in **i**. Statistical significance was determined by unpaired two-sided *t*-test ($n = 3$ technical replicates). **k**, Slot blot of 293T *TERC*$^{-/-}$ cells transfected as in **i** and treated with the indicated dose of dT, 5FU (10 μM) or hydroxyurea (HU; 500 μM), as indicated. Representative data from one of two biological replicates are displayed. **l**, Quantification of **k**, as in **j** ($n = 3$ technical replicates). The data in **b**, **f**, **j** and **l** are presented as means and error bars indicate s.d. Full-length gels are provided as source data.

repeat synthesis by telomerase, these experiments could not distinguish substrate-dependent versus substrate-independent effects of dTTP on telomerase activity. To study this further, we engineered a modified *TERC* expression vector with the template region encoding T-free (GGAAAG) repeats rather than wild-type (GGTTAG) repeats (Fig. 7c), allowing us to interrogate potential substrate-independent

effects of dTTP on telomerase activity. When we tested T-free super-telomerase cell extracts in a modified TRAP assay (Extended Data Fig. 7c,d), we found increased T-free telomerase activity with increasing dTTP levels (Extended Data Fig. 7e–h). Sequencing T-free telomerase TRAP products demonstrated that dT was not represented in the extended products (Extended Data Fig. 7i–k). These results confirmed that T-free telomerase does not use dTTP as a substrate, and surprisingly suggested a substrate-independent effect of dTTP on telomerase activity. To determine this without the potential confounder of PCR amplification in the TRAP assay, we directly tested the effects of dTTP on immunopurified T-free telomerase, as measured by incorporation of [α-^{32}P]-dATP on a telomere repeat oligonucleotide substrate[55]. Remarkably, dTTP enhanced T-free telomerase activity in a dose-dependent manner (Fig. 7d), with levels approximately 50% higher at a concentration of 25 µM (Fig. 7e,f), and with a greater effect on longer telomerase products suggestive of increased telomerase processivity (Extended Data Fig. 7l). Taken together, these results show that dTTP is capable of increasing telomerase activity in a manner independent of its role as a substrate, potentially through an allosteric mechanism.

Substrate-independent control of telomerase in cells by dT

After observing this substrate-independent effect of dTTP on telomerase activity in vitro, we next asked whether dT treatment could enhance T-free super-telomerase activity in cells. When we transfected *TERC*-null 293T cells with *TERT* and T-free *TERC* vectors, we detected altered repeat sequences on native telomere ends by PCR (Fig. 7g,h). Southern blot analysis showed increases in telomerase-dependent GGAAAG signals in response to dT. However, these signals appeared over a range of molecular weights rather than just elongation of pre-existing telomere ends as seen with the native GGTTAG template (Extended Data Fig. 7m,n). This might be explained by instability of an unprotected G-rich GGAAAG repeat extension, which likely cannot be bound by POT1, cannot undergo C-strand fill-in due to the requirement for polymerase alpha/primase to begin the RNA primer with a purine[56,57] (templated by C or T, now absent from the T-free G-rich strand) and cannot efficiently complement the native telomere sequence to form a T-loop, and is thus potentially subject to nucleolytic cleavage. Nevertheless, to quantify T-free telomerase repeat synthesis in cells, we used slot blotting to measure GGAAAG repeat content in cellular DNA (Extended Data Fig. 7o–r) and found a specific increase in GGAAAG repeats in cells overexpressing T-free super-telomerase (Fig. 7i,j). When we treated cells overexpressing wild-type versus T-free super-telomerase with 100 µM dT, we found an increase in GGAAAG repeat content exclusively in cells expressing T-free telomerase (Fig. 7i,j and Extended Data Fig. 7s,t). Furthermore, we found that treatment with 5FU or hydroxyurea decreased levels of GGAAAG repeats in T-free super-telomerase-expressing cells and that treatment with dT could rescue the inhibition of GGAAAG repeat synthesis following 5FU treatment (Fig. 7k,l)—patterns identical to those found with the native template (Fig. 6m). These findings support a model wherein dTTP increases telomerase activity in human cells by a mechanism independent of its role as a telomerase substrate.

Thymidine manipulation elongates telomeres in patient induced pluripotent stem cells

TBDs are caused by mutations in at least 18 genes[12,35] regulating telomere maintenance. We asked whether treatment with dT or disruption of *SAMHD1* could promote telomere lengthening in induced pluripotent stem cells (iPSCs) derived from patients with TBDs. We first confirmed that dT supplementation for 3 weeks significantly elongated telomeres in iPSCs from a healthy donor (Fig. 8a,b). Next, we tested a panel of iPSCs from patients with TBDs with hypomorphic genetic defects, including mutations in *TERC*, *DKC1* (encoding a component of the telomerase holoenzyme) or *PARN*, the product of which promotes TERC maturation. We found that treatment with 50 µM dT for 3 weeks produced telomere elongation in all cases (Fig. 8a,b). When we examined the impact of dT treatment on cell cycle progression in iPSCs, we found that doses ≤50 µM had minimal effects (Extended Data Fig. 8a,b). Assessment of pCHK1-S345 and pRPA32-S33 by immunoblotting revealed no indication of replication stress signaling in iPSCs upon treatment with dT (Extended Data Fig. 8c), in line with previous literature[58]. Next, we evaluated the capacity of stable *SAMHD1* knockdown to alter telomere length in both wild-type iPSCs and patient iPSCs harboring TBD-causing mutations (including in the genes *DKC1*, *PARN* and *TINF2*, which encodes a telomere shelterin component) and found telomere elongation across the genotypes tested (Fig. 8c–e). Collectively, these data show that manipulation of thymidine nucleotide metabolism can restore telomere lengthening in stem cells harboring TBD-causing genetic defects.

Discussion

Impaired telomere length maintenance is associated with reduced lifespan[9] and fatal genetic degenerative diseases[10–12,59]. Using phenotypic CRISPR–Cas9 screening in intact cells, we identified thymidine nucleotide metabolism as a critical pathway controlling human telomere length homeostasis. DNA precursor levels are tightly controlled though a balance of de novo synthesis, salvage and catabolism[13]. Here we demonstrate that telomere length is highly sensitive to changes in thymidine nucleotide metabolism (Fig. 8f and Extended Data Fig. 9): loss of genes in the thymidine nucleotide synthesis or salvage pathways decreased telomere length, whereas loss of the dNTP-degrading gene *SAMHD1* lengthened telomeres. In addition to genetic perturbations, we found that telomere synthesis is highly sensitive to small molecules targeting thymidine nucleotide metabolism. Supplementing cells with dT drove robust telomere elongation, whereas treatment with 5FU or hydroxyurea, which limit dTTP production, blocked telomere repeat synthesis by telomerase. Collectively, our work, in line with emerging population and Mendelian genetic data[9,34,35], demonstrates the critical importance of thymidine nucleotide metabolism in human telomere length control and highlights the additional insights gained from longitudinal functional genetic studies in human cells.

While dTTP is a canonical substrate of human telomerase alongside dATP and dGTP, this striking impact of thymidine nucleotide metabolism on telomere length in human cells is unexpected given previous studies using reconstituted telomerase[19,20,23,24] and yeast[60,61] indicating that dGTP is rate limiting for telomerase activity. Here, using a modified telomerase enzyme that no longer uses dTTP as a substrate, we found evidence for substrate-independent enhancement of telomerase activity by dT nucleotides both in vitro and in living cells. While we cannot exclude a role for secondary effects of dT on dATP and dGTP levels contributing to telomere length changes in cells, a substrate-independent, potentially allosteric effect of dTTP on telomerase activity offers a unifying mechanism to explain our genetic, pharmacological and biochemical findings that, coupled with recent human genetic data[9,34,35], firmly establishes a role for thymidine nucleotide metabolism in telomere length regulation. More specifically, a preponderance of orthogonal evidence, including high-throughput functional genetic screening, 5FU treatment, GWASs and genetic discovery, collectively implicates *TYMS* as a critical control point, thus revealing a limiting role for de novo dT nucleotide production in human telomere length regulation.

Previous work connected replication stress signaling with enhanced telomerase recruitment to telomeres[52] and increased telomere length[51,53]. Our data show that telomere lengthening from dT can occur at doses that do not result in replication stress or disrupt the cell cycle. Furthermore, we showed that 5FU and hydroxyurea—compounds known to cause replication stress—blocked telomere repeat synthesis by telomerase in our system, rather than extending telomeres. We cannot exclude that replication stress-mediated changes in telomerase recruitment could play a role in telomere elongation at very high dT

https://doi.org/10.1038/s41588-023-01339-5

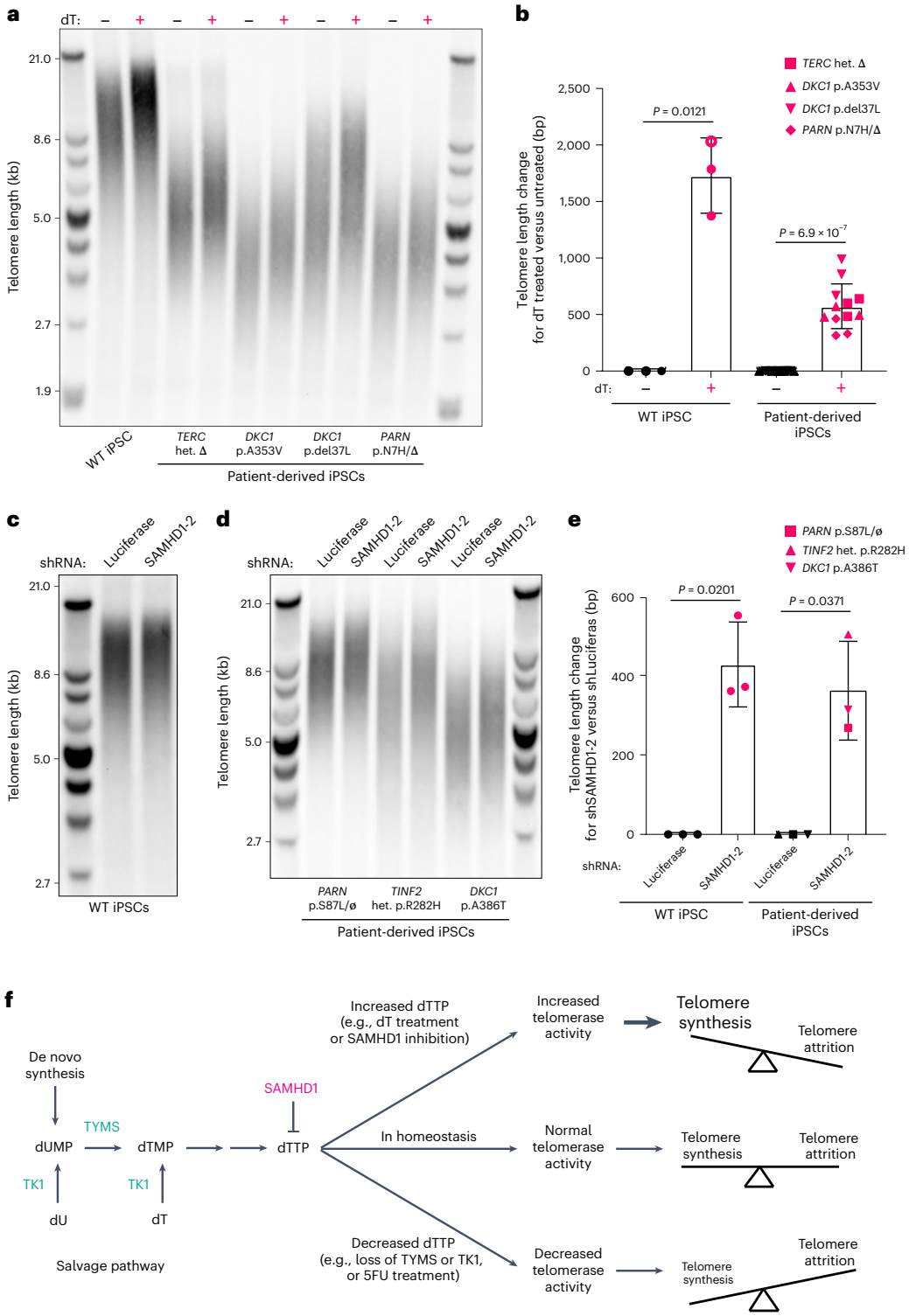

Fig. 8 | dT supplementation or SAMHD1 knockdown drives telomere lengthening in iPSCs from patients with TBDs. a, TRF of iPSCs derived from a healthy donor or from TBD patients harboring mutations in the indicated genes that were treated with or without 50 µM dT for 3 weeks. A representative blot from three biological replicates is shown. **b**, Quantification of **a**. Statistical significance was determined by paired two-sided *t*-test. The open circle indicates treatment with 100 µM dT for 3 weeks. All other treated cells received 50 µM dT. All data points represent biologically independent samples. Sample sizes were as follows: $n = 3$ for wild-type iPSCs either untreated or treated with dT and $n = 12$ for iPSCs derived from patients with TBD, either untreated or treated with dT. **c**, TRF of wild-type iPSCs transduced with the indicated shRNA expression construct and cultured for 26 d. A representative blot from three biological replicates is shown. **d**, TRF of iPSCs derived from TBD patients harboring mutations in the indicated genes that were transduced with the indicated shRNA expression construct and cultured for 1 month. **e**, Quantification of **c** and **d**, as in **b**. All of the data points represent biologically independent samples. Sample sizes were as follows: $n = 3$ samples for wild-type iPSCs transduced with shLuciferase or shSAMHD1-2 and $n = 3$ samples for patient-derived iPSCs transduced with shLuciferase or shSAMHD1-2. **f**, Model of the relationship between dTTP metabolism and telomere length. The data in **b** and **e** are presented as means and error bars indicate s.d.

doses; however, our data clearly show that modulating dT nucleotides at more physiological levels can impact human telomere length by other means, such as activation of telomerase.

While we show that cell cycle inhibition and replication stress cannot explain telomere lengthening from dT, we found that the high doses of dT commonly used to synchronize cells cause substantial changes in telomere repeat synthesis. Several investigations of human telomerase biology have used dT or related compounds such as bromodeoxyuridine to facilitate measurements such as the timing of telomere synthesis by telomerase during the cell cycle, and the kinetics of repeat addition by telomerase at a given chromosome end. Our results indicate that a more nuanced interpretation of telomere biology effects may be required when using dT and its analogs for synchronization or labeling in human cells.

Defects of nucleotide synthesis are associated with diseases, including mitochondrial genetic disorders and cancer[13–15], and manipulation of nucleotide metabolism is widely used in life-saving therapies, including those for cancer and autoimmune and infectious diseases[62,63]. Remarkably, we found that supplementation with dT promotes rapid telomere lengthening at low micromolar doses. We observed this effect across various cell lines, including iPSCs derived from patients with TBDs caused by diverse, hypomorphic genetic defects. Based on our findings in vitro and in cultured cells, along with promising clinical trials currently underway using oral dT supplementation to treat a mitochondrial genetic disease[64], we propose that there may be a therapeutic window to modulate telomere length via manipulating thymidine metabolism in patients with a range of genetic degenerative disorders.

dNTP metabolism is commonly considered in relation to DNA replication and repair. Our work uncovers a unique sensitivity of telomerase reverse transcriptase activity to thymidine nucleotide homeostasis. While dT supplementation alone can inhibit genome replication by DNA polymerases[49] and human immunodeficiency virus type 1 reverse transcription[65], we found that dT treatment drove robust increases in telomere synthesis by telomerase. These findings expand our understanding of how differences in the common pool of cellular nucleotide substrates driven by genetic variation and other factors can have distinct effects on the various DNA synthesis machineries in the cell. Evolutionary pressures on dNTP metabolism have likely faced a trade-off between telomere length maintenance, nuclear and mitochondrial genomic integrity and other forces, including the restriction of endogenous or exogenous retroelements. Telomere length homeostasis offers a new lens with which to examine the genetic regulation and evolution of DNA precursor metabolism in humans.

Online content

Any methods, additional references, Nature Portfolio reporting summaries, source data, extended data, supplementary information, acknowledgements, peer review information; details of author contributions and competing interests; and statements of data and code availability are available at https://doi.org/10.1038/s41588-023-01339-5.

References

1. Fagagna, F. et al. A DNA damage checkpoint response in telomere-initiated senescence. *Nature* **426**, 194–198 (2003).
2. Takai, H., Smogorzewska, A. & de Lange, T. DNA damage foci at dysfunctional telomeres. *Curr. Biol.* **13**, 1549–1556 (2003).
3. Olovnikov, A. M. A theory of marginotomy: the incomplete copying of template margin in enzymic synthesis of polynucleotides and biological significance of the phenomenon. *J. Theor. Biol.* **41**, 181–190 (1973).
4. Watson, J. D. Origin of concatemeric T7 DNA. *Nat. New Biol.* **239**, 197–201 (1972).
5. Harley, C. B., Futcher, A. B. & Greider, C. W. Telomeres shorten during ageing of human fibroblasts. *Nature* **345**, 458–460 (1990).
6. Greider, C. W. & Blackburn, E. H. Identification of a specific telomere terminal transferase activity in tetrahymena extracts. *Cell* **43**, 405–413 (1985).
7. Greider, C. W. & Blackburn, E. H. A telomeric sequence in the RNA of *Tetrahymena* telomerase required for telomere repeat synthesis. *Nature* **337**, 331–337 (1989).
8. Feng, J. et al. The RNA component of human telomerase. *Science* **269**, 1236–1241 (1995).
9. Codd, V. et al. Polygenic basis and biomedical consequences of telomere length variation. *Nat. Genet.* **53**, 1425–1433 (2021).
10. Armanios, M. & Blackburn, E. H. The telomere syndromes. *Nat. Rev. Genet.* **13**, 693–704 (2012).
11. Niewisch, M. R. & Savage, S. A. An update on the biology and management of dyskeratosis congenita and related telomere biology disorders. *Expert Rev. Hematol.* **12**, 1037–1052 (2019).
12. Revy, P., Kannengiesser, C. & Bertuch, A. A. Genetics of human telomere biology disorders. *Nat. Rev. Genet.* **24**, 86–108 (2023).
13. Mathews, C. K. Deoxyribonucleotide metabolism, mutagenesis and cancer. *Nat. Rev. Cancer* **15**, 528–539 (2015).
14. Buj, R. & Aird, K. M. Deoxyribonucleotide triphosphate metabolism in cancer and metabolic disease. *Front. Endocrinol.* **9**, 177 (2018).
15. El-Hattab, A. W. & Scaglia, F. Mitochondrial DNA depletion syndromes: review and updates of genetic basis, manifestations, and therapeutic options. *Neurotherapeutics* **10**, 186–198 (2013).
16. Meuth, M., L'Heureux-Huard, N. & Trudel, M. Characterization of a mutator gene in Chinese hamster ovary cells. *Proc. Natl Acad. Sci. USA* **76**, 6505–6509 (1979).
17. Weinberg, G., Ullman, B. & Martin, D. W. Mutator phenotypes in mammalian cell mutants with distinct biochemical defects and abnormal deoxyribonucleoside triphosphate pools. *Proc. Natl Acad. Sci. USA* **78**, 2447–2451 (1981).
18. Schaich, M. A. et al. Mechanisms of nucleotide selection by telomerase. *eLife* **9**, e55438 (2020).
19. Maine, I. P., Chen, S. F. & Windle, B. Effect of dGTP concentration on human and CHO telomerase. *Biochemistry* **38**, 15325–15332 (1999).
20. Sun, D., Lopez-Guajardo, C. C., Quada, J., Hurley, L. H. & Von Hoff, D. D. Regulation of catalytic activity and processivity of human telomerase. *Biochemistry* **38**, 4037–4044 (1999).
21. Chen, Y., Podlevsky, J. D., Logeswaran, D. & Chen, J. J.-L. A single nucleotide incorporation step limits human telomerase repeat addition activity. *EMBO J.* **37**, e97953 (2018).
22. Hwang, H., Opresko, P. & Myong, S. Single-molecule real-time detection of telomerase extension activity. *Sci. Rep.* **4**, 6391 (2014).
23. Hardy, C. D., Schultz, C. S. & Collins, K. Requirements for the dGTP-dependent repeat addition processivity of recombinant *Tetrahymena* telomerase. *J. Biol. Chem.* **276**, 4863–4871 (2001).
24. Hammond, P. W. & Cech, T. R. dGTP-dependent processivity and possible template switching of euplotes telomerase. *Nucleic Acids Res.* **25**, 3698–3704 (1997).
25. Doench, J. G. et al. Optimized sgRNA design to maximize activity and minimize off-target effects of CRISPR–Cas9. *Nat. Biotechnol.* **34**, 184–191 (2016).
26. Baerlocher, G. M., Vulto, I., de Jong, G. & Lansdorp, P. M. Flow cytometry and FISH to measure the average length of telomeres (flow FISH). *Nat. Protoc.* **1**, 2365–2376 (2006).
27. Alder, J. K. et al. Diagnostic utility of telomere length testing in a hospital-based setting. *Proc. Natl Acad. Sci. USA* **115**, E2358–E2365 (2018).
28. Li, W. et al. MAGeCK enables robust identification of essential genes from genome-scale CRISPR/Cas9 knockout screens. *Genome Biol.* **15**, 554 (2014).

29. De Lange, T. Shelterin: the protein complex that shapes and safeguards human telomeres. *Genes Dev.* **19**, 2100–2110 (2005).
30. Loayza, D. & de Lange, T. POT1 as a terminal transducer of TRF1 telomere length control. *Nature* **423**, 1013–1018 (2003).
31. Lee, T. H. et al. Essential role of Pin1 in the regulation of TRF1 stability and telomere maintenance. *Nat. Cell Biol.* **11**, 97–105 (2009).
32. O'Connor, M. S., Safari, A., Liu, D., Qin, J. & Songyang, Z. The human Rap1 protein complex and modulation of telomere length. *J. Biol. Chem.* **279**, 28585–28591 (2004).
33. Wang, B. et al. Integrative analysis of pooled CRISPR genetic screens using MAGeCKFlute. *Nat. Protoc.* **14**, 756–780 (2019).
34. Li, C. et al. Genome-wide association analysis in humans links nucleotide metabolism to leukocyte telomere length. *Am. J. Hum. Genet.* **106**, 389–404 (2020).
35. Tummala, H. et al. Germline thymidylate synthase deficiency impacts nucleotide metabolism and causes dyskeratosis congenita. *Am. J. Hum. Genet.* **109**, 1472–1483 (2022).
36. Reichard, P. Interactions between deoxyribonucleotide and DNA synthesis. *Ann. Rev. Biochem.* **57**, 349–374 (1988).
37. Martínez-Arribas, B. et al. DCTPP1 prevents a mutator phenotype through the modulation of dCTP, dTTP and dUTP pools. *Cell. Mol. Life Sci.* **77**, 1645–1660 (2020).
38. Goldstone, D. C. et al. HIV-1 restriction factor SAMHD1 is a deoxynucleoside triphosphate triphosphohydrolase. *Nature* **480**, 379–382 (2011).
39. Franzolin, E. et al. The deoxynucleotide triphosphohydrolase SAMHD1 is a major regulator of DNA precursor pools in mammalian cells. *Proc. Natl Acad. Sci. USA* **110**, 14272–14277 (2013).
40. Powell, R. D., Holland, P. J., Hollis, T. & Perrino, F. W. Aicardi–Goutieres syndrome gene and HIV-1 restriction factor SAMHD1 is a dGTP-regulated deoxynucleotide triphosphohydrolase. *J. Biol. Chem.* **286**, 43596–43600 (2011).
41. Jamburuthugoda, V. K., Chugh, P. & Kim, B. Modification of human immunodeficiency virus type 1 reverse transcriptase to target cells with elevated cellular dNTP concentrations. *J. Biol. Chem.* **281**, 13388–13395 (2006).
42. Yuan, M., Breitkopf, S. B., Yang, X. & Asara, J. M. A positive/negative ion-switching, targeted mass spectrometry-based metabolomics platform for bodily fluids, cells, and fresh and fixed tissue. *Nat. Protoc.* **7**, 872–881 (2012).
43. Lahouassa, H. et al. SAMHD1 restricts HIV-1 by reducing the intracellular pool of deoxynucleotide triphosphates. *Nat. Immunol.* **13**, 223–228 (2012).
44. Majerska, J., Feretzaki, M., Glousker, G. & Lingner, J. Transformation-induced stress at telomeres is counteracted through changes in the telomeric proteome including SAMHD1. *Life Sci. Alliance* **1**, e201800121 (2018).
45. Daddacha, W. et al. SAMHD1 promotes DNA end resection to facilitate DNA repair by homologous recombination. *Cell Rep.* **20**, 1921–1935 (2017).
46. Coquel, F. et al. SAMHD1 acts at stalled replication forks to prevent interferon induction. *Nature* **557**, 57–61 (2018).
47. Beloglazova, N. et al. Nuclease activity of the human SAMHD1 protein implicated in the Aicardi–Goutières syndrome and HIV-1 restriction. *J. Biol. Chem.* **288**, 8101–8110 (2013).
48. Morris, E. R. et al. Crystal structures of SAMHD1 inhibitor complexes reveal the mechanism of water-mediated dNTP hydrolysis. *Nat. Commun.* **11**, 3165 (2020).
49. Xeros, N. Deoxyriboside control and synchronization of mitosis. *Nature* **194**, 682–683 (1962).
50. Bootsma, D., Budke, L. & Vos, O. Studies on synchronous division of tissue culture cells initiated by excess thymidine. *Exp. Cell Res.* **33**, 301–309 (1964).
51. Lee, S. S., Bohrson, C., Pike, A. M., Wheelan, S. J. & Greider, C. W. ATM kinase is required for telomere elongation in mouse and human cells. *Cell Rep.* **13**, 1623–1632 (2015).
52. Tong, A. S. et al. ATM and ATR signaling regulate the recruitment of human telomerase to telomeres. *Cell Rep.* **13**, 1633–1646 (2015).
53. Sfeir, A. et al. Mammalian telomeres resemble fragile sites and require TRF1 for efficient replication. *Cell* **138**, 90–103 (2009).
54. Cristofari, G. & Lingner, J. Telomere length homeostasis requires that telomerase levels are limiting. *EMBO J.* **25**, 565–574 (2006).
55. Morin, G. B. The human telomere terminal transferase enzyme is a ribonucleoprotein that synthesizes TTAGGG repeats. *Cell* **59**, 521–529 (1989).
56. Yamaguchi, M., Hendrickson, E. A. & DePamphilis, M. L. DNA primase-DNA polymerase alpha from simian cells: sequence specificity of initiation sites on simian virus 40 DNA. *Mol. Cell. Biol.* **5**, 1170–1183 (1985).
57. Roth, Y.-F. Eucaryotic primase. *Eur. J. Biochem.* **165**, 473–481 (1987).
58. Desmarais, J. A., Unger, C., Damjanov, I., Meuth, M. & Andrews, P. Apoptosis and failure of checkpoint kinase 1 activation in human induced pluripotent stem cells under replication stress. *Stem Cell Res. Ther.* **7**, 17 (2016).
59. Tummala, H., Walne, A. & Dokal, I. The biology and management of dyskeratosis congenita and related disorders of telomeres. *Expert Rev. Hematol.* **15**, 685–696 (2022).
60. Gupta, A. et al. Telomere length homeostasis responds to changes in intracellular dNTP pools. *Genetics* **193**, 1095–1105 (2013).
61. Maicher, A. et al. Rnr1, but not Rnr3, facilitates the sustained telomerase-dependent elongation of telomeres. *PLoS Genet.* **13**, e1007082 (2017).
62. Jordheim, L. P., Durantel, D., Zoulim, F. & Dumontet, C. Advances in the development of nucleoside and nucleotide analogues for cancer and viral diseases. *Nat. Rev. Drug Discov.* **12**, 447–464 (2013).
63. Broen, J. C. A. & van Laar, J. M. Mycophenolate mofetil, azathioprine and tacrolimus: mechanisms in rheumatology. *Nat. Rev. Rheumatol.* **16**, 167–178 (2020).
64. Domínguez-González, C. et al. Deoxynucleoside therapy for thymidine kinase 2-deficient myopathy. *Ann. Neurol.* **86**, 293–303 (2019).
65. Meyerhans, A. et al. Restriction and enhancement of human immunodeficiency virus type 1 replication by modulation of intracellular deoxynucleoside triphosphate pools. *J. Virol.* **68**, 535–540 (1994).

Methods

Human study participants

Biological samples were procured under Boston Children's Hospital Institutional Review Board-approved protocols, after written informed consent in accordance with the Declaration of Helsinki. Patients and patient-derived iPSCs were as described[66–68]. The patient with mutation of the *TINF2* gene presented with dyskeratosis congenita and bone marrow failure in early childhood, consistent with the pathognomonic mutation leading to the p.Arg282His amino acid change.

Cell culture

K562 cells (American Type Culture Collection (ATCC)) were grown in RPMI1640 (Gibco) media supplemented with 10% fetal bovine serum. 293T cells (ATCC) were grown in Dulbecco's Modified Eagle Medium (Gibco) supplemented with 10% fetal bovine serum, and were subcultured using 0.05% trypsin (Gibco). iPSCs were grown in Essential 8 Medium (Life Technologies) supplemented with ROCK Inhibitor Y-271632 (STEMCELL Technologies) at 10 µM on plates coated with human embryonic stem cell-qualified Matrigel matrix (Corning) and were subcultured using Accutase (STEMCELL Technologies). The iPSC line with mutation of *TINF2* was derived from bone marrow-derived fibroblasts using the 4-in-1-dTomato lentiviral reprogramming vector (a kind gift from A. Schambach) as described[69]. The iPSCs with mutation of *PARN* were derived and characterized as described[66]. The iPSC line with mutation of *DKC1* transcribing the p.Ala353Val variant was derived and characterized as described[68]. The iPSCs with mutations in *DKC1* transcribing the p.del37Leu and p.Ala386Thr variants were derived and characterized as described[67]. The iPSC line with mutation of *TERC* was derived and characterized as described[67]. The wild-type iPSC line was derived and characterized as described[66].

Lentiviral transduction of shRNA and overexpression constructs was performed in media supplemented with protamine sulfate (Sigma–Aldrich) at 10 µg ml^{-1} for 16 h. Transduced cells underwent selection with puromycin (Sigma–Aldrich) at 2 µg ml^{-1} for 3–5 d or blasticidin (InvivoGen) at 10 µg ml^{-1} for 5–10 d. For doxycycline-inducible transgene expression, 1 µg ml^{-1} doxycycline (Sigma–Aldrich) was used.

Transfections were performed using Lipofectamine LTX with Plus Reagent (Invitrogen) in Opti-MEM (Gibco) according to the manufacturers' instructions. On the evening before transfection, 2 million cells were plated per well of a six-well dish, then transfected with 2.5 µg total DNA per well. pXPR_011 was used as the eGFP control vector, pBS U3-TERC-500 was used to overexpress TERC and PCDNA3.1-3XHA-TERT was used to overexpress TERT. For conditions under which TERT was transfected in addition to TERC/eGFP, the total DNA input was kept the same and a 5:1 mass ratio of TERC to TERT vector was used. Unless otherwise stated, super-telomerase extracts were generated using cells 2 d post-transfection.

Quantification of cell growth was performed using hemocytometry with Trypan Blue viability staining. For growth curves, 50,000 cells were plated per well in a 12-well dish, or 100,000 cells were plated per well in a six-well dish. Cells were passaged when subconfluent, counted using a hemocytometer and replated at equal numbers in fresh media.

Lentivirus production

293T cells were transfected with psPAX2 and pMD2.G, as well as the appropriate transfer vector by calcium phosphate precipitation. Virus-containing media was harvested 48 and 72 h after transfection. shRNA and overexpression construct virus-containing media was filtered with 0.45-µm filters (VWR International) and stored at −80 °C. For sgRNA libraries, virus-containing media was filtered using 0.45-µm filters and concentrated by ultracentrifugation followed by resuspension in Dulbecco's Modified Eagle Medium and storage at −80 °C.

Cas9-expressing cell line generation and validation

K562 cells (ATCC) were transduced with lentivirus containing the Lenti-Cas9-2A-Blast construct followed by selection in 10 µg ml^{-1} blasticidin for 10 d. After selection, cells were transduced with the pXPR_011 vector and cultured for 2 weeks followed by flow cytometry to quantify the percentage of GFP-positive cells on an LSR II analyzer (BD Biosciences) using BD FACSDiva version 8.0.2. Cells were gated using forward scatter and side scatter gating, as described in Extended Data Fig. 1d, using FlowJo version 10.7.1.

sgRNA library design and production

For secondary screening using a nucleotide metabolism-focused sgRNA library, genes were selected for inclusion based on annotated involvement in nucleotide salvage and deoxyribonucleotide metabolism by Gene Ontology. Ten sgRNAs per gene were designed using the Broad GPP sgRNA Design tool[25,70]. A total of 200 nontargeting sgRNA sequences were selected from the Brunello sgRNA library. Library information, including genes targeted and sgRNA sequences, can be found in Supplementary Table 1. A pool of single-stranded DNA encoding the sgRNAs flanked by BsmBI recognition sites and overhang sequences for PCR amplification (as described[70]) was synthesized by Twist Bioscience. The library was PCR amplified using Q5 High-Fidelity Taq Polymerase (NEB) and cloned into lentiGuide-Puro using Golden Gate cloning[70] with BsmBI-v2 (NEB) and T4 DNA Ligase (NEB) in T4 DNA Ligase Buffer (NEB). The library was transformed into chemically competent Stbl3 cells (Invitrogen), which were prepared using the Mix & Go! *E. coli* Transformation Kit (Zymo Research). Sufficient transformation reactions were performed to attain >40 colonies per sgRNA. Library representation was confirmed by PCR amplification using Titanium Taq DNA Polymerase (Takara Bio), followed by next-generation sequencing using an Illumina MiSeq instrument and library quantification using the MAGeCK RRA[28] software. Gene-specific and nontargeting sgRNA libraries were cloned separately and pooled in appropriate quantities to maximize sgRNA representation before lentivirus production.

Flow-FISH telomere length and CRISPR–Cas9-based screening

Cas9-expressing K562 cells were plated at 3 million cells per well in 12-well dishes at numbers sufficient for >3,000× library coverage. Cells were spinfected at 931*g* for 2 h at 30 °C in 1 ml media per well, in the presence of 10 µg ml^{-1} protamine sulfate (Sigma–Aldrich). After the spin, 3 ml fresh media was added and cells were incubated overnight. Virus was removed on day 1. Puromycin selection at 2 µg ml^{-1} was performed from days 2–6. Sufficient virus was used to ensure that between 20 and 50% of cells were infected. After puromycin selection, cells were cultured at >1,000× library coverage for the indicated amount of time. Flow-FISH was performed using an Alexa 647-conjugated TelC-PNA probe (PNA Bio) as described[26,71]. Cells were counterstained with 4′,6-diamidino-2-phenylindole (DAPI) and gated on DAPI low cells and then based on Alexa 647 fluorescence, as described in Extended Data Fig. 1. Cells were sorted using either a BD FACSAria II or a FACSAria III. For the Brunello library, 200 million cells on each day were sorted using the above method on days 49 and 50 from the same population of cells. Samples from the two days were treated as replicates for downstream analysis. For the nucleotide metabolism sgRNA library experiment, approximately 20 million cells were sorted from two populations that had been infected and cultured separately, and were treated as replicates for downstream analysis. Gates were adjusted throughout the sort such that approximately 5% of cells with the highest and lowest Alexa 647 fluorescence were collected. DNA from sorted cells was purified by phenol–chloroform extraction using standard procedures. Next, sgRNAs were PCR amplified using Titanium Taq DNA Polymerase (Takara Bio) and primers containing Illumina P5 and P7 binding sites[70]. PCR products were purified using a 1:1 ratio of sample purification SPRI magnetic beads (Beckman Coulter). Pooled, barcoded amplicons were sequenced on an Illumina NextSeq using

75-bp high-output chemistry. Data analysis and quality control were performed using the MAGeCKFlute pipeline (version 0.5.9.2)[33]. Briefly, FASTQ files were mapped using the count function with the control norm-method. Gene enrichment scores were calculated using the test function comparing the low Alexa 647 versus high Alexa 647 (Fig. 1b) populations for the nucleotide metabolism targeted library, or high Alexa 647 versus unsorted (Extended Data Fig. 1h) and low Alexa 647 versus unsorted (Extended Data Fig. 1i) populations for the Brunello library, with the MAGeCK RRA using paired replicates and nontargeting guides as controls. Unbiased pathway analysis was performed using the hypergeometic test to identify KEGG pathways enriched using the FluteRRA function, which includes *q* value estimation for false discovery rate control.

Detailed information regarding cell sorting and library quality and a gene significance score table for the Brunello library can be found in Supplementary Tables 2–5.

Terminal restriction fragment length analysis

Genomic DNA was isolated from cells using the PureLink Genomic DNA Mini Kit (Invitrogen). In brief, 1–3 µg gDNA was digested with RsaI (NEB) and HinfI (NEB) for 2–3 h at 37 °C and loaded onto a 0.6% agarose gel followed by Southern blotting onto Hybond-N+ membrane (Amersham). Then, detection was performed using the TeloTAGGG Telomere Length Assay Kit (Roche) with either the telomeric probe provided in the kit or an GGAAAG complementary probe, which was synthesized as described[72] using the GGAAAG Probe Template oligonucleotide (see below). GGAAAG complementary probe was used at a working concentration of 1 ng ml^{-1} DIG Easy Hyb (Roche). After hybridization, detection was performed as described in the TeloTAGGG Telomere Length Assay Kit (Roche). Probed membranes were stripped by briefly rinsing in water then washing twice with 0.2 M NaOH and 0.1% sodium dodecyl sulfate (SDS) at 37 °C for 15 min with shaking, followed by hybridization and detection as described above. Quantification was performed using the WALTER webtool[73]. Statistical analysis was performed using GraphPad Prism version 9.1.0.

RNA isolation and reverse transcription quantitative real-time PCR

RNA was isolated from cells using TRIzol Reagent (Invitrogen). RNA was DNAse treated with the TURBO DNA-free Kit (Invitrogen). Complementary DNA was synthesized using SuperScript III Reverse Transcriptase (Invitrogen) using random hexamers (Invitrogen). Quantitative PCR was performed using SsoAdvanced Universal SYBR Green Supermix (Bio-Rad) in technical triplicates. Relative expression was quantified using ΔΔCt methodology.

TRAP assay

Cell extracts for TRAP assays were made using TRAPeze 1X CHAPS Lysis Buffer (Roche) supplemented with RNasin (Promega). Standard TRAP reactions (in Fig. 7a and Extended Data Fig. 2) were performed as described[74], with cell input normalized across samples using the Bio-Rad DC assay. TRAP assays were modified to enable unique dNTP concentrations in telomerase reactions from PCR reactions (in Fig. 7d,e and Extended Data Fig. 7a–f) as follows. Reactions were assembled with 1× TRAP buffer (20 mM Tris-HCl (pH 8.3), 1.5 mM $MgCl_2$, 63 mM KCl, 0.05% Tween 20 and 1 mM EGTA), TS, ACX, TNST and NT primers as described[74] (see the section 'Primers and oligonucleotides' below). dNTPs were added at physiologic concentrations (24 µM dATP, 5.2 µM dGTP, 29 µM dCTP and 37 µM dTTP)[75] unless otherwise mentioned in the figure legends, followed by telomerase extracts. TRAP assays were modified to detect GGAAAG repeats using the following primers: TS GGAAAG, TNST GGAAAG, ACX GGAAAG and NT (see the section 'Primers and oligonucleotides' below). After the addition of telomerase extracts, reactions were incubated for 30 min at 30 °C, followed by heat inactivation at 95 °C for 5 min. Reactions were purified to remove dNTPs using the Oligo Clean and Concentrator Kit (Zymo Research) and eluted in 15 µl water. Then, 10 µl elutate was used in TRAP PCR reactions along with 1× TRAP buffer, 0.4 U Titanium Taq DNA Polymerase and 50 µM of each dNTP, and PCR was performed as described[74]. PCR products were resolved on 10% polyacrylamide gels (Bio-Rad), stained with GelRed (Biotium) and imaged on a Bio-Rad ChemiDoc Touch imager. Images were quantified for a given lane using ImageJ by measuring the signal of the telomerase repeat-sized products divided by the signal of the internal control band for the lane, normalized to the same ratio for the untreated sample(s) in a given experiment[74]. Statistical analysis was performed using GraphPad Prism version 9.1.0.

Targeted CRISPR–Cas9 gene editing

For targeted CRISPR–Cas9 gene editing, 37 pmol Alt-R S.p. Cas9 Nuclease V3 (Integrated DNA Technologies) and 50 pmol chemically modified sgRNA(s) (Synthego) were complexed at room temperature for 20 min. Then, 200,000–400,000 cells were combined with Cas9/gRNA complexes in 20 µl Buffer R (Thermo Fisher Scientific) with Alt-R Cas9 Electroporation Enhancer (Integrated DNA Technologies), followed by electroporation using the Neon Transfection System (Thermo Fisher Scientific) and the Neon Transfection 10 µl Kit. K562 cells were electroporated with three pulses at 1,150 V for 10 ms. 293T cells were electroporated with one pulse of 1,200 V for 30 ms.

CRISPR–Cas9 gene editing efficiency determination

Genomic DNA was isolated from cells using the PureLink Genomic DNA Mini Kit (Invitrogen), followed by PCR amplification with Q5 High-Fidelity DNA Polymerase (NEB) with the High GC Enhancer, followed by either running on a 2% agarose gel or Sanger sequencing. Sanger trace files were analyzed using the Synthego ICE webtool version 3.0 to calculate the editing efficiency. The editing efficiency was determined using the same DNA used for terminal restriction fragment (TRF) blotting.

Cell cycle analysis by DNA content staining and flow cytometry

Cells were prepared either for flow-FISH staining as described[26] (for experiments in Extended Data Fig. 5) or by ethanol fixation (for the data in Fig. 6 and Extended Data Figs. 6 and 8), followed by rehydration and counterstaining using DAPI (BD Biosciences) and analysis on an LSR II or LSRFortessa analyzer (BD Biosciences) using BD FACSDiva 8.0.2. Cells were gated using forward versus side scatter gating, as described in Extended Data Fig. 1d, using FlowJo version 10.7.1.

Immunoblotting

For the immunoblots in Fig. 6 and Extended Data Fig. 8, cells were lysed in RIPA buffer (150 mM NaCl, 1% Triton X-100, 0.5% sodium deoxycholate, 0.1% SDS and 50 mM Tris (pH 8.0)) supplemented with HALT Protease Inhibitor Cocktail (Thermo Fisher Scientific) and quantified using the Bio-Rad DC assay, then 10 µg lysate was combined with 2× Laemmli sample buffer (Bio-Rad) and run on a 10% SDS-PAGE gel (Bio-Rad) followed by transfer to a polyvinylidene difluoride membrane (Bio-Rad) using standard procedures. For the immunoblots in Extended Data Fig. 4, cells were lysed in 1× Laemmli sample buffer (Bio-Rad) and run on a 10% SDS-PAGE gel (Bio-Rad), followed by transfer to a polyvinylidene difluoride membrane (Bio-Rad) using standard procedures. Human SAMHD1 was detected using primary antibody from either Abcam (ab67820; Extended Data Fig. 6a,c) or Origene (OTI3F5; Extended Data Fig. 6b) at 1:500 dilution and horseradish peroxidase-conjugated goat-anti-mouse IgG H&L (ab205719) at 1:1,000 dilution. pCHK1-S345 was detected using a rabbit monoclonal primary antibody from Cell Signaling Technology (133D3) at 1:1,000 dilution. pRPA32-S33 was detected using a rabbit primary antibody from Bethyl Laboratories (A300-246A) at 1:1,000 dilution. Rabbit primary antibodies were detected using horseradish peroxidase-conjugated goat-anti-rabbit IgG H&L antibody (1706515; Bio-Rad) at 1:3,000

dilution. Anti-beta-actin antibody directly conjugated to horseradish peroxidase (C4; sc-47778 HRP; Santa Cruz Biotechnology) at 1:1,000 was used to quantify relative loading. Imaging was performed using a Bio-Rad ChemiDoc imager.

Liquid chromatography–mass spectrometry

Extraction and quantification of polar metabolites was performed as described[42] using high-performance liquid chromatography-grade methanol (Fisher Scientific). If a given species was detected in multiple ion modes, the mode with the highest average signal in the untreated cells was used for analysis.

Nanopore sequencing

For sequencing of telomere end PCR products (Fig. 7h,i), amplicons were purified using the Qiagen PCR Purification Kit and sequenced using the Plasmidsaurus amplicon sequencing service. Data from Plasmidsaurus nanopore sequencing and Sanger sequencing were aligned and displayed using Geneious Prime. T-free TRAP products were prepared for nanopore sequencing using the Ligation Sequencing Kit with the Native Barcoding Expansion (SQK-LSK109 and EXP-NBD104; Oxford Nanopore Technologies) according to the manufacturer's instructions, except that a ratio of 4:1 of SPRI Purification Beads (Beckman Coulter) was used for all purification steps. Samples were pooled after barcode ligation and adapters were ligated per the manufacturer's instructions, then products were loaded onto a Flongle Flow Cell (FLO-FLG001). Reads were first analyzed using the high-accuracy mode (MinKNOW/Guppy) and reads that had passed quality standards (Q score > 9) from the high-accuracy base calling were re-base called using the super-high-accuracy algorithm (MinKNOW/Guppy). Then, super-high-accuracy base-called reads that had a Q score of >10 were used for further analysis. Read counts and quality metrics are provided in Supplementary Table 6. FASTQ files were analyzed in MATLAB as follows. Reads containing a match to the TS GGAAAG forward primer and the TAGGGAT portion of the reverse primer reverse complement were extracted and the base pairs between the primer binding sites were analyzed for their base pair composition using version 1.0 of a custom MATLAB script that has been posted to the public repository[76] (also see Extended Data Fig. 7i diagram). The software versions used were Geneious Prime 2019.2.3, MinKNOW 22.05.5, Bream 7.1.3, Configuration 5.1.5, Guppy 6.1.5, MinKNOW Core 5.1.0 and MATLAB R2021a. Base pair frequency analysis and the plotting in Extended Data Fig. 7h,i were performed using ggseqlogo[77] with R version 4.1.2.

Telomerase immunopurification

293T *TERC*-null cells were transfected as described above with 3xHA-TERT and TERC/eGFP in 10-cm-diameter dishes with reagents scaled up in proportion to the cell growth area. Two days after transfection, cells were harvested, washed once in phosphate-buffered saline and lysed in TRAPeze 1X CHAPS Lysis Buffer (Roche) supplemented with RNasin Plus (Promega) and HALT Protease Inhibitor Cocktail (Thermo Fisher Scientific), followed by incubation on ice for 30 min and precipitation of insoluble material by centrifugation. Immunoprecipitation was performed as described at https://www.colorado.edu/lab/cech/lab-protocols with minor modifications. Briefly, 75 µl anti-HA magnetic beads (SAE0197; Sigma–Aldrich; mouse IgG1 monoclonal antibody; clone HA-7; 50% beads by volume) were added to clarified lysates followed by 2 h incubation at 4 °C while rotating. Before addition, beads were prepared by washing four times in 50 mM Tris-HCl (pH 8.0), 1 mM $MgCl_2$, 1 mM spermidine and 5 mM β-mercaptoethanol. After immunoprecipitation, telomerase-bound beads were washed four times with 1 ml telomerase buffer with 30% glycerol (50 mM Tris-HCl (pH 8.0), 50 mM KCl, 1 mM $MgCl_2$, 1 mM spermidine, 5 mM β-mercaptoethanol and 30% glycerol). After washing, a 50% bead slurry was made with telomerase buffer with 30% glycerol, then the beads were aliquoted, snap frozen and stored at −80 °C.

Direct telomerase assay

Reactions were performed as described at https://www.colorado.edu/lab/cech/lab-protocols with minor modifications. 20 µl reactions were assembled containing 6 µl immunopurified telomerase, 5.2 µM dGTP, 3 µM dATP, 0.166 µM [α-^{32}P]-dATP (3,000 Ci mmol^{-1}; PerkinElmer), 1 µM PAGE-purified 3×(TTAGGG) primer (Integrated DNA Technologies), 50 mM Tris-HCl (pH 8.0), 50 mM KCl, 1 mM $MgCl_2$, 1 mM spermidine and 5 mM β-mercaptoethanol. dTTP was added as indicated. Reactions were then incubated at 30 °C for 1 h, then 100 µl stop buffer (3.6 M ammonium acetate and 10 mg ml^{-1} glycogen) was added as well as ^{32}P-end-labeled PAGE-purified TTAGGGTTAGGGTTAG primer (Integrated DNA Technologies) followed by the addition of 500 µl ethanol. Products were then incubated at −80 °C for 45 min, pelleted, washed with 1 ml 70% ethanol, dried and resuspended in 10 µl water. Purified products were combined 1:1 with electrophoresis buffer (0.1× TBE, 50 mM EDTA, 0.1% bromophenol blue, 0.1% xylene cyanol and 93% formamide), denatured at 95 °C for 5 min and then centrifuged at 18,000g for 5 min to precipitate insoluble material. 9 µl of samples were then loaded onto 10% acrylamide/7 M urea gels. After electrophoresis, gels were then dried using the Bio-Rad GelAir Drying System and imaged using phosphorimaging on an Amersham Typhoon 5 Biomolecular Imager (GE Healthcare). End labeling of the loading control primer was performed using T4 Polynucleotide Kinase (NEB) and [γ-^{32}P]-dATP (6,000 Ci mmol^{-1}; PerkinElmer). Images were quantified using ImageJ as follows. For total telomerase activity measurement (Fig. 7f), the telomerase product signal in a lane was quantified and normalized to the loading control band signal within the same lane. This ratio was then normalized to the average product-to-loading control ratio for the 0 µM dTTP lanes. For the analysis of telomerase repeat intensity (Extended Data Fig. 7l), the signal of each repeat (defined as the three consecutive intense bands in the laddering pattern, as indicated in Fig. 7d) was quantified and first normalized to the loading control band signal for that lane. Then, the ratio of a given repeat to loading control was divided by the corresponding ratio for the 0 µM dTTP lane, yielding a measure of relative repeat intensity, which was plotted for repeats 1–4. Statistical analysis was performed using GraphPad Prism version 9.1.0.

Slot blotting

Slot blotting was performed as described[78] with minor modifications. Briefly, the DNA concentration was normalized to 20 ng µl^{-1} using a nanodrop spectrophotometer. 3.3 µl DNA was added to 16.5 µl denaturation solution (0.5 M NaOH and 1.5 M NaCl) and heated to 55 °C for 30 min. 495 µl neutralization solution (0.5 M Tris-HCl and 1.5 M NaCl) was added to denatured DNA and 156 µl of this solution was added in triplicate to different slots on a Bio-Dot SF Apparatus (Bio-Rad) and blotted onto a Hybond-N+ Membrane (Cytivia). Membrane preparation and washing were performed as described[78]. For samples with paired GGTTAG and GGAAAG slot blots, the above recipe was doubled and 156 µl was loaded onto parallel membranes in triplicate on each membrane. After blotting, membranes were hybridized and detected as described above for TRF Southern blots using the indicated probe. Blots were analyzed using ImageJ. Statistical analysis was performed using GraphPad Prism version 9.1.0.

shRNA construct cloning

Oligonucleotides encoding shRNAs targeting SAMHD1 or luciferase control were annealed and cloned into the pLKO.1-puro vector using the Quick Ligation Kit (NEB).

Expression construct cloning

SAMHD1 expression constructs were cloned using primers with flanking attB sites to amplify the *SAMHD1* sequence derived from complementary DNA prepared as described above or eGFP from the pXPR-011 vector using Q5 High-Fidelity DNA Polymerase (NEB). Amplicons were

cloned into the pCW57.1 vector in a single reaction using Gateway LR Clonase II Enzyme mix (Invitrogen), Gateway BP Clonase II Enzyme mix (Invitrogen) and the Gateway pDONR221 Vector (Invitrogen). Point mutations were introduced using the Q5 Site-Directed Mutagenesis Kit (NEB) and verified using Sanger sequencing. The T-free TERC construct was generated using the Q5 Site-Directed Mutagenesis Kit (NEB) and verified using Sanger sequencing.

Plasmids

The 4-in-1-dTomato lentiviral reprogramming vector was a gift from A. Schambach. Lenti-Cas9-2A-Blast was a gift from J. Moffat (plasmid 73310; Addgene). pXPR_011 was a gift from J. Doench and D. Root (plasmid 59702; Addgene). The human Brunello CRISPR knockout pooled library in lentiGuide-Puro was a gift from D. Root and J. Doench (73178; Addgene). lentiGuide-Puro was a gift from F. Zhang (plasmid 52963; Addgene). The pLKO.1-TRC cloning vector was a gift from D. Root (plasmid 10878; Addgene). pCW57.1 was a gift from D. Root (plasmid 41393; Addgene). psPAX2 was a gift from D. Trono (plasmid 12260; Addgene). pMD2.G was a gift from D. Trono (plasmid 12259; Addgene). pBS U3-hTR-500 was a gift from K. Collins (plasmid 28170; Addgene). pCDNA-3xHA-hTERT was a gift from S. Artandi (plasmid 51637).

Nucleoside and other small molecules

Please see Supplementary Table 7 for information regarding the source and quality of nucleosides and other small molecules used in this study.

Primers and oligonucleotides

All oligonucleotides were manufactured by Integrated DNA Technologies. Primer sequence information can be found in Supplementary Table 8.

Reporting summary

Further information on research design is available in the Nature Portfolio Reporting Summary linked to this article.

Data availability

The sgRNA library sequencing data and T-free TRAP sequencing data used for analysis have been deposited in the Sequence Read Archive and are available via BioProject accession code PRJNA851386. Source data are provided with this paper.

Code availability

The MATLAB script used to analyze the T-free TRAP sequencing data has been posted to a public repository[76]. Version 1.0 was used in this manuscript (https://doi.org/10.5281/zenodo.7607615).

References

66. Moon, D. H. et al. Poly(A)-specific ribonuclease (PARN) mediates 3′-end maturation of the telomerase RNA component. *Nat. Genet.* **47**, 1482–1488 (2015).
67. Agarwal, S. et al. Telomere elongation in induced pluripotent stem cells from dyskeratosis congenita patients. *Nature* **464**, 292–296 (2010).
68. Paulsen, B. S. et al. Ectopic expression of RAD52 and dn53BP1 improves homology-directed repair during CRISPR–Cas9 genome editing. *Nat. Biomed. Eng.* **1**, 878–888 (2017).
69. Warlich, E. et al. Lentiviral vector design and imaging approaches to visualize the early stages of cellular reprogramming. *Mol. Ther.* **19**, 782–789 (2011).
70. Sanson, K. R. et al. Optimized libraries for CRISPR–Cas9 genetic screens with multiple modalities. *Nat. Commun.* **9**, 5416 (2018).
71. Nagpal, N. et al. Small-molecule PAPD5 inhibitors restore telomerase activity in patient stem cells. *Cell Stem Cell* **26**, 896–909.e8 (2020).
72. Lai, T.-P., Wright, W. E. & Shay, J. W. Generation of digoxigenin-incorporated probes to enhance DNA detection sensitivity. *Biotechniques* **60**, 306–309 (2016).
73. Lyčka, M. et al. WALTER: an easy way to online evaluate telomere lengths from terminal restriction fragment analysis. *BMC Bioinformatics* **22**, 145 (2021).
74. Herbert, B.-S., Hochreiter, A. E., Wright, W. E. & Shay, J. W. Nonradioactive detection of telomerase activity using the telomeric repeat amplification protocol. *Nat. Protoc.* **1**, 1583–1590 (2006).
75. Traut, T. W. Physiological concentrations of purines and pyrimidines. *Mol. Cell. Biochem.* **140**, 1–22 (1994).
76. Mannherz, W. TRAP nanopore analysis. *Zenodo* https://doi.org/10.5281/zenodo.7607615 (2023).
77. Wagih, O. ggseqlogo: a versatile R package for drawing sequence logos. *Bioinformatics* **33**, 3645–3647 (2017).
78. Kimura, M. & Aviv, A. Measurement of telomere DNA content by dot blot analysis. *Nucleic Acids Res.* **39**, e84 (2011).

Acknowledgements

We thank the patients and families for research participation. We thank R. Mathieu and the Harvard Stem Cell Institute (HSCI)-Boston Children's Hospital (BCH) Flow Cytometry Research Lab; the Molecular Biology Core Facilities at the Dana-Farber Cancer institute (for high-throughput sequencing support); J. Asara and the Beth Israel Deaconess Medical Center Mass Spectrometry Core Facility; and A. Shimamura, M. Fleming and the BCH Bone Marrow Failure/Myelodysplastic Syndrome Registry (National Institutes of Health (NIH) grant R21DK099808). We thank L. Zon and Y. Fong for critical input. We thank A. Gutierrez and K. Bodaar for guidance and support with the CRISPR–Cas9 screening. We thank D. Moon for generating the *TERC*-null 293T cell line. We acknowledge the following funding sources: NIH grants T32GM007226, T32GM007753 and T32GM144273 (to W.M.), NIH grants R01DK107716 and R33HL154133 (to S.A.), the BCH Translational Research Program, HSCI, Team Telomere, the Million Dollar Bike Ride/Penn Medicine Orphan Disease Center and philanthropic gifts (to S.A.). This content is solely the responsibility of the authors and does not necessarily represent the official views of the National Institutes of Health.

Author contributions

S.A. and W.M. conceived of the study and designed the experiments. W.M. performed the experiments and analyzed the data. S.A. and W.M. wrote the manuscript.

Competing interests

S.A. and W.M. are named as inventors on provisional patent application 63/394,588 relating to the data shown.

Additional information

Extended data is available for this paper at https://doi.org/10.1038/s41588-023-01339-5.

Supplementary information The online version contains supplementary material available at https://doi.org/10.1038/s41588-023-01339-5.

Correspondence and requests for materials should be addressed to Suneet Agarwal.

Peer review information *Nature Genetics* thank Jens Schmidt, Tracy Bryan and the other, anonymous, reviewer(s) for their contribution to the peer review of this work.

https://doi.org/10.1038/s41588-023-01339-5

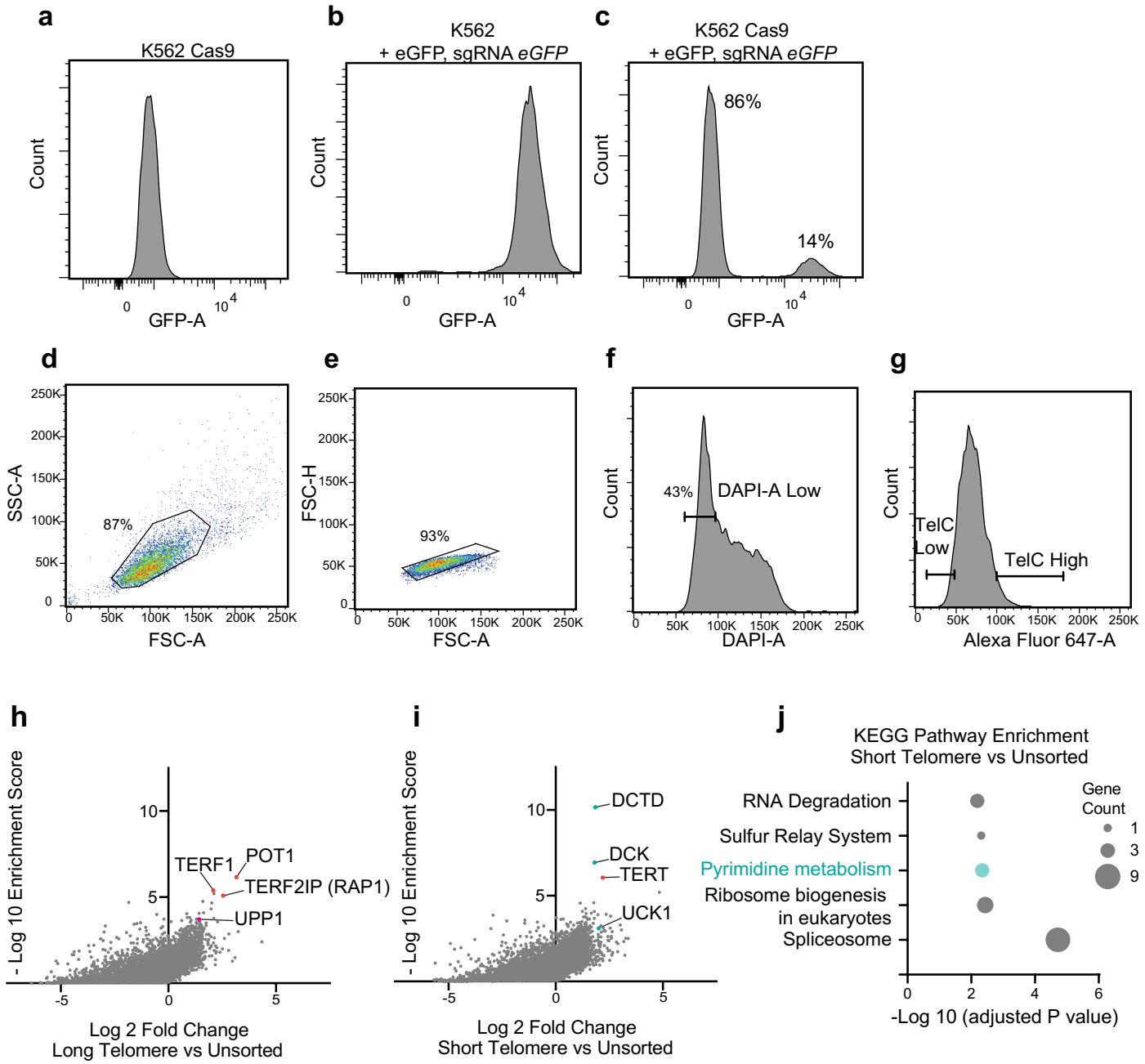

Extended Data Fig. 1 | Telomere length CRISPR/Cas9 screening using flow-FISH. a-**c**, Histogram of GFP fluorescence from K562 cells (**a**), K562 cells transduced with the pXPR-011 vector which expresses eGFP and an sgRNA targeting eGFP (**b**), and K562 cells expressing Cas9 and transduced with the pXPR-011 vector, 13 days post transduction (**c**). Presence of GFP-negative cells in **c** indicates functional Cas9 nuclease activity. **d**-**g**, Representative gating strategy for flow-FISH telomere length screening. Data from nucleotide metabolism library infected K562 cells, replicate 1. Cells are gated to enrich for single cells (**e**, **f**), and gated on low DAPI fluorescence to enrich for cells with 2 N genome copy number and aid in identifying sgRNAs which promote telomere elongation independent from changes in total DNA content (**g**) followed by gating on high and low TelC-Alexa 647 probe fluorescence populations. Gates adjusted to maintain approximately 5% of cells throughout the duration of the sort. **h**, **i**, sgRNA enrichment in high (**h**) and low (**i**) telomere fluorescence populations compared to unsorted populations from K562 cells expressing Cas9 that were infected with the Brunello sgRNA library and then cultured for 49 days followed by flow-FISH sorting of the 5% of cells with the highest and lowest telomere fluoresence in two replicates performed on consecutive days. Enrichment score calculated using the MAGeCK RRA software. Known telomere length regulating genes indicated with orange dots; other genes indicated are involved in nucleotide metabolism. **j**, KEGG pathway enrichment analysis performed on the genes with sgRNAs enriched in the sorted short telomere population (**i**), analysis performed using the MAGeCKFlute software package (see Methods). Plot includes top enriched KEGG terms, plotting -$\log_{10}$ adjusted *P* value, which includes *q*-value estimation for false discovery rate control; dot size indicates number of genes identified in that pathway out of the short telomere enriched genes.

https://doi.org/10.1038/s41588-023-01339-5

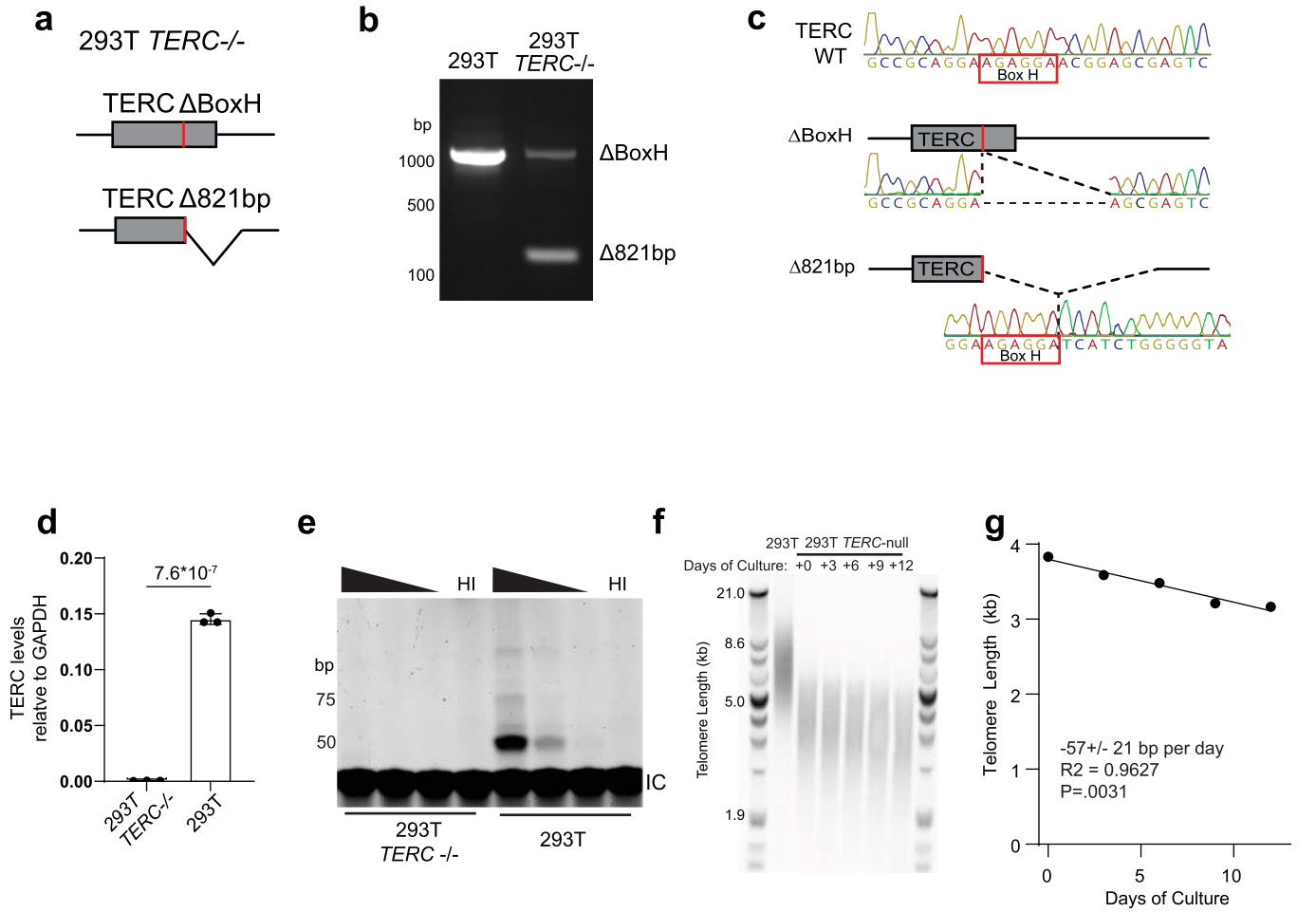

Extended Data Fig. 2 | Characterization of *TERC*-null 293T cells. a, Schematic of *TERC* genotypes in TERC-null 293T cells generated by genome-editing, including a deletion of the essential box H domain on one allele, and an 821-bp *TERC* locus deletion that encompasses 74 bp from the 3' end of *TERC* on the other allele. **b**, Ethidium bromide stained agarose gel of PCR of 293T or 293T *TERC*-null genomic DNA using primers flanking the deletions indicated in **a**. **c**, Sanger sequencing of gel-purified PCR products from the (1) higher molecular weight bands in **b**, indicating that the non-deleted allele lacks the box H domain, and (2) the Δ821 bp deleted band from **b**, with trace file showing the deletion junction in a genomic context. **d**, RT-qPCR of *TERC* expression relative to *GAPDH* in wild-type 293T and *TERC*-null 293T cells, performed in technical triplicate. *P* value calculated by unpaired *t* test. Data are shown are means and error bars indicate standard deviation. **e**, Telomerase activity measured via the TRAP assay, performed on 5-fold serial dilutions of lysates. HI indicates heat-inactivated lysate. IC indicates the internal control product. **f**, TRF of wild-type and *TERC*-null 293T cells. Days of culture were recorded beginning approximately two months after gene editing. Telomere length gradually declines with passage until cells universally senesce. **g**, Quantification of **f**, line fit using simple linear regression. Data presented in this figure are the results of single experiments unless otherwise indicated.

https://doi.org/10.1038/s41588-023-01339-5

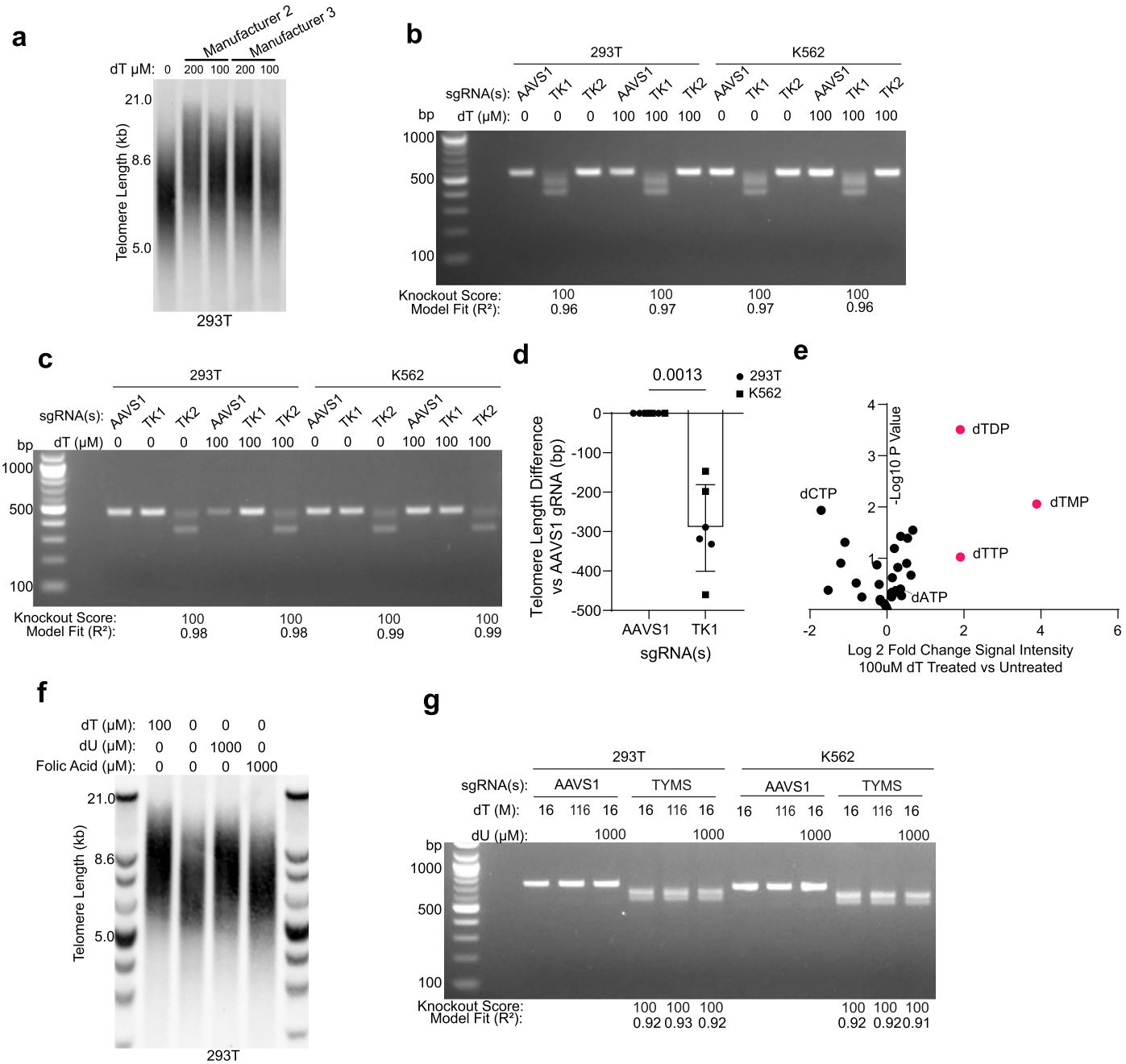

Extended Data Fig. 3 | dT nucleotide metabolism perturbations and their effects on telomere length and polar metabolite homeostasis. a, TRF of 293T cells treated with the indicated dose of dT for 10 days. The 0 µM dT lane is the same image as the rightmost lane in Fig. 2f. Manufacturer 2, Santa Cruz Biotechnology; Manufacturer 3, MP Biomedicals. **b**,**c**, Genomic DNA from 293T or K562 cells manipulated with the indicated sgRNA(s) followed by dT treatment was PCR amplified using primers specific to the *TK1* (**b**) or *TK2* (**c**) genomic loci. Amplicons were separated by agarose gel electrophoresis, demonstrating the three pooled sgRNAs targeting either *TK1* or *TK2* generated on-target genomic deletions. First lane is a molecular weight marker. PCR products were Sanger sequenced and editing efficiency was quantified using the Synthego ICE algorithm (shown as 'Knockout Score'). The model fit of the ICE quantification is also displayed. Genomic DNA used in this figure was the same as the DNA used to generate Fig. 3b–e. **d**, Quantification of Fig. 3b. $n = 3$ biological replicates for each cell line, P value calculated using paired two-sided t test. **e**, Polar metabolite profiling by liquid chromatography mass spectrometry of 293 T cells treated with or without 100 µM dT for 24 hours, performed in biological triplicate. P value calculated by unpaired two-sided Student's t test of average signal intensity in treatment vs. control samples; nucleotide and nucleoside species detected in all samples displayed. Note: dGTP not detected. **f**, TRF of 293T cells treated with the indicated compound for 10 days. dU, deoxyuridine. **g**, Detection of CRISPR/Cas9 editing of *TYMS* locus using *TYMS*-specific primers, performed as in **b** and **c**. Genomic DNA used was the same as the DNA used to generate data in Fig. 3g–j. Data in **d** and **e** are shown as means, and error bars indicate standard deviation.

https://doi.org/10.1038/s41588-023-01339-5

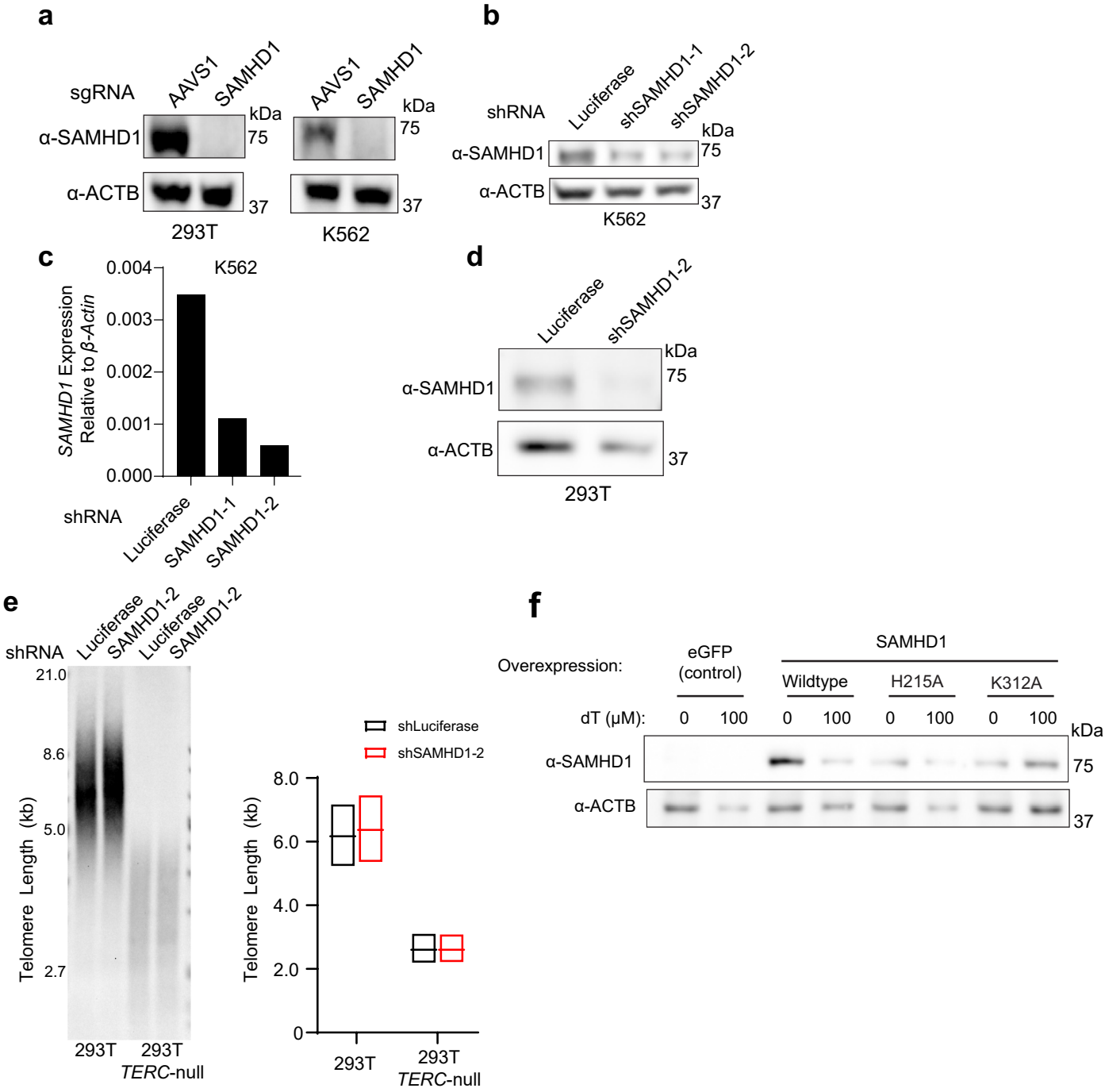

Extended Data Fig. 4 | Manipulation of SAMHD1 levels by CRISPR/Cas9, shRNA, and lentiviral expression. a, Immunoblot of 293T and K562 cells electroporated with Cas9 and the indicated sgRNA(s) using primary antibodies against SAMHD1 or β-Actin, corresponding to cell lines evaluated in Fig. 4b. **b**, Immunoblot of K562 cells transduced with vectors expressing the indicated shRNA, corresponding to cell lines evaluated in Fig. 4c. **c**, qRT-PCR of SAMHD1 expression compared to β-Actin, performed in technical triplicate. Means of the replicates are shown. **d**, Immunoblot of 293T cells transduced with vectors expressing the indicated shRNA. **e**, TRF of indicated cell lines transduced with the indicated shRNA and cultured for 15 days, and quantification of the TRF using the WALTER webtool. The boxplot displays the 75th, 50th and 25th percentile molecular weight of the telomere signal distribution in the TRF blot. **f**, Immunoblot of 293T cells transduced with vectors to overexpress either eGFP or the indicated SAMHD1 variant and treated with the indicated dose of dT, corresponding to cell lines evaluated in Fig. 4i, j. Data presented in this figure are the results of single experiments unless otherwise stated. Full-length western blots are presented as source data.

https://doi.org/10.1038/s41588-023-01339-5

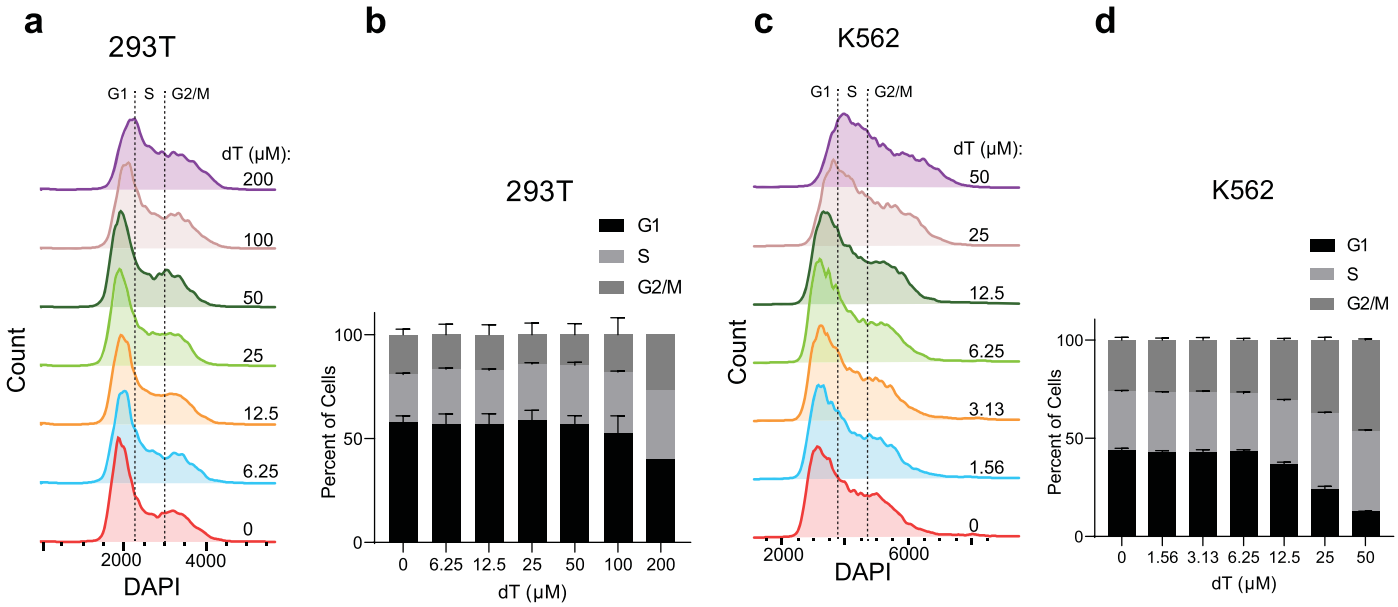

Extended Data Fig. 5 | Cell cycle assessment of cells treated with dT. a–d, DAPI staining of 293T (**a**, **b**) and K562 (**c**, **d**) cells treated with the indicated dose of dT for 7 or 8 days, respectively, measured by flow cytometry, plotted as histograms of DAPI intensity, displaying representative samples from each treatment arm (**a**, **c**), and the percentage of cells in different stages of the cell cycle (**b**, **d**) gated based on the lines drawn on the histogram, gates determined based on untreated samples. $n = 2$ biological replicates for 293T cells treated with 200 μM dT and $n = 3$ biological replicates for all other conditions. Data presented are means; error bars indicate standard deviation.

https://doi.org/10.1038/s41588-023-01339-5

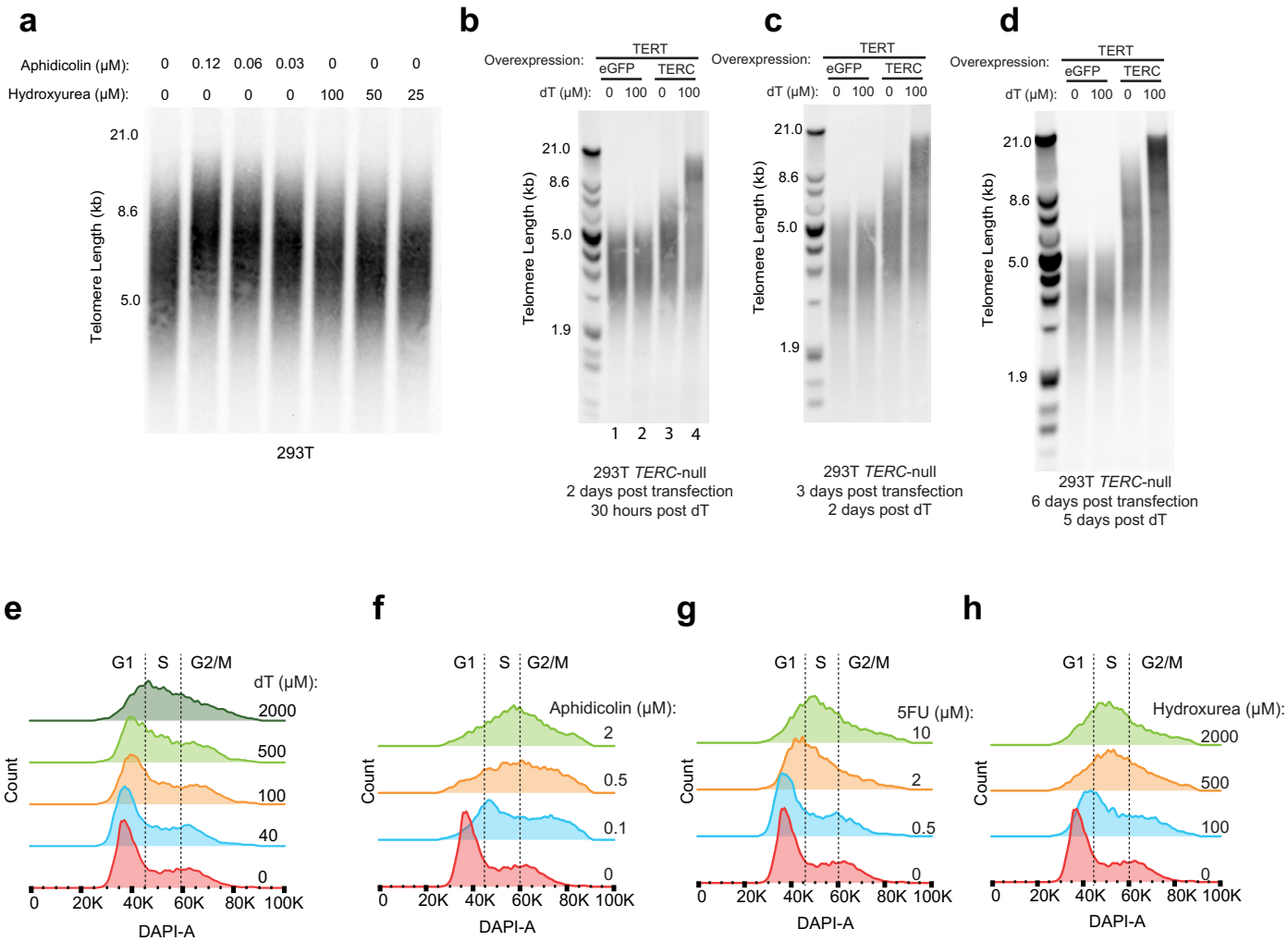

Extended Data Fig. 6 | Evaluation of telomere length and cell cycle progression changes from treatment with dT, aphidicolin, 5FU, or hydroxyurea. a, TRF Southern blot of 293T cells treated with the indicated doses of aphidicolin and hydroxyurea for 10 days. **b**, TRF Southern blot of 293T *TERC*-null cells transfected with *TERT* in addition to the indicated vector, cultured for 18 hours, then treated with the indicated dose of dT for 30 hours. **c**, TRF Southern blot of 293T *TERC*-null cells transfected with *TERT* in addition to the indicated vector, cultured for 18 hours, then treated with the indicated dose of dT for two days. **d**, TRF Southern blot of 293T *TERC*-null cells transfected with the indicated expression vectors, cultured for 18 hours, then treated with the indicated dose of dT for five days. **e**–**h**, Cell cycle analysis by DAPI staining and flow cytometry of 293T *TERC*-null cells transfected with *TERC* and *TERT* expression vectors, cultured for 18 hours, then treated with the indicated of dose of dT (**e**), aphidicolin (**f**), 5FU (**g**), or hydroxyurea (**h**), displayed as histograms of DAPI intensity of representative samples from each treatment arm, corresponding to cells in Fig. 6b–l. Gating based on untreated cells. TRFs presented in this figure show the results of single experiments.

https://doi.org/10.1038/s41588-023-01339-5

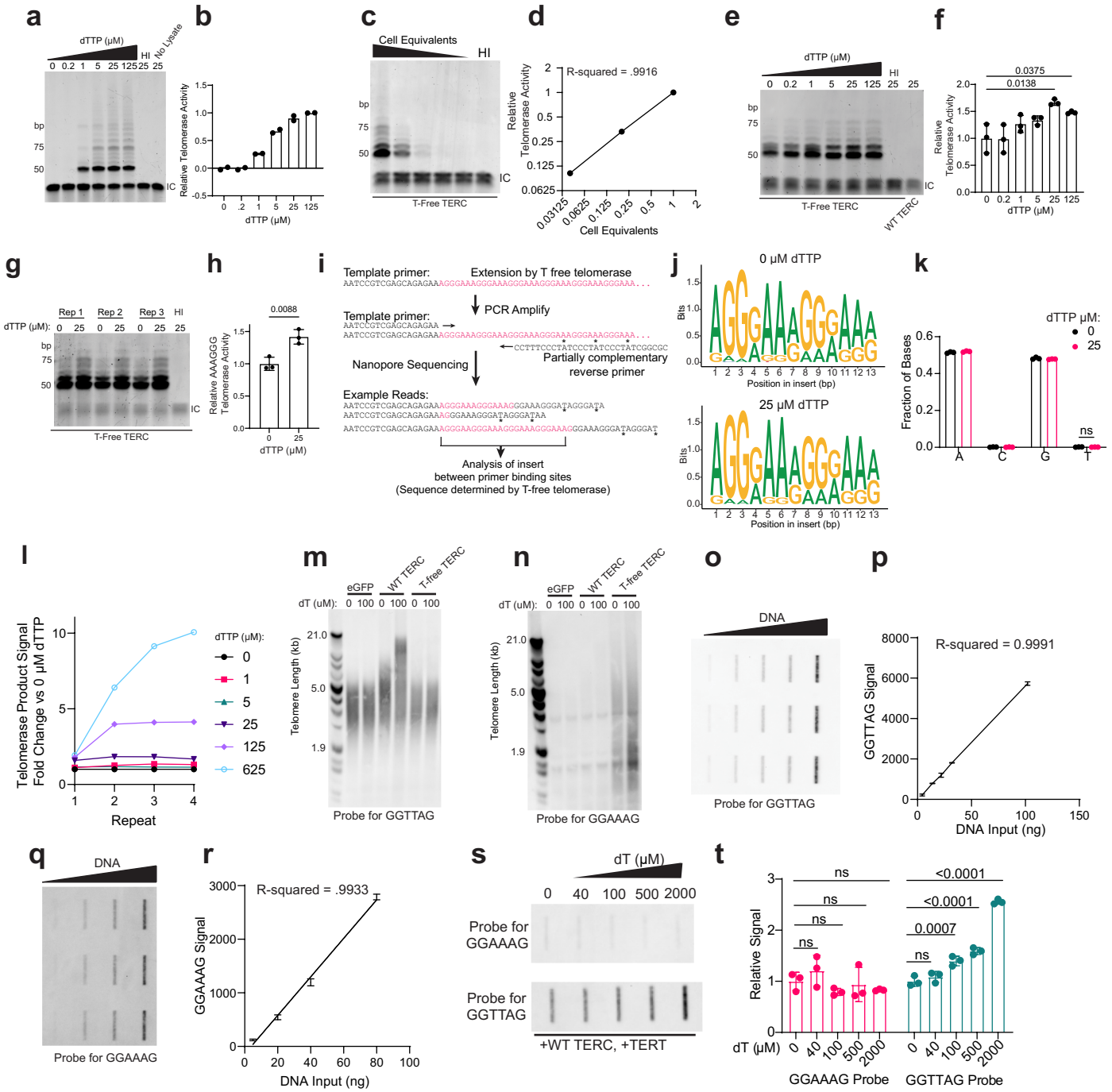

Extended Data Fig. 7 | See next page for caption.

https://doi.org/10.1038/s41588-023-01339-5

Extended Data Fig. 7 | T-free telomerase is sensitive to dT nucleotide manipulations. a, Representative modified TRAP assay performed on super-telomerase extracts using the indicated dose of dTTP and physiologic levels of dATP, dCTP and dGTP (see Methods). **b**, Quantification of **a**. $n = 2$ biological replicates. **c**, GGAAAG TRAP assay performed on lysates from 293T *TERC*-null cells overexpressing T-free super-telomerase demonstrates linearity between cell input amount and telomerase signal. Five-fold serial dilutions performed. HI, heat inactivated. **d**, Quantification of lanes 1–3 from **c**. **e**, Representative modified GGAAAG TRAP assay performed on super-telomerase extracts generated using the indicated *TERC* vector. Assay performed with the indicated dose of dTTP and physiologic levels of dATP, dCTP and dGTP (see Methods). HI, heat inactivated. **f**, Quantification of **e** using two-sided unpaired Student's *t* test; $n = 3$ biological replicates. **g**, Representative modified GGAAAG TRAP assay performed on T-free super-telomerase extracts supplemented with the indicated dose of dTTP and physiologic levels of dATP and dGTP. **h**, Quantification of **g** as in **f**, $n = 3$ biological replicates. **i**, Diagram of GGAAAG TRAP product sequencing and analysis strategy. Note * indicates T's encoded by the partially complementary reverse primer, preventing analysis of base composition in that portion of the read. **j**, Quantification of base pair composition of representative GGAAAG TRAP products from **g** with 0 µM or 25 µM dTTP by nanopore sequencing (see Methods). Bits of information calculated using Shannon entropy and plotted using ggseqlogo. **k**, Quantification of base pair composition of GGAAAG TRAP products from **g** using nanopore sequencing (see Methods). *P* value calculated using two-sided Student's *t* test; $n = 3$ biological replicates. **l**, Quantification of Fig. 7d, plotting the signal in the indicated telomerase product repeat relative to the signal of the corresponding repeat in the lane without dTTP added, normalized for loading (see Methods). **m**, TRF Southern blot of 293T *TERC*-null cells transfected with *TERT* in addition to the indicated vector, cultured for 18 hours, then treated with the indicated dose of dT for 30 hours, and probed with a GGTTAG complementary probe. Lanes 1–4 are the same blot shown in Extended Data Fig. 6b. **n**, Blot from **m** was stripped and re-probed with a probe complementary to the GGAAAG repeat. **o**, Slot blot of DNA from 293T *TERC*-null cells overexpressing eGFP and TERT showing linear relationship between DNA input and signal; rows are technical triplicates. **p**, Quantification of **o**. **q**, Slot blot of DNA from 293T *TERC*-null cells overexpressing T-free super-telomerase; rows are technical triplicates. **r**, Quantification of **q**. **s**, Slot blot of DNA from 293T-*TERC* null cells transfected with *TERT* and *TERC*, cultured for 18 hours, then treated with dT as indicated for 30 hours. Denatured DNA for each sample was split and loaded onto parallel blots, which were probed for the indicated target. Performed in technical triplicate. **t**, Quantification of **s**. *P* values calculated with one way ANOVA using Dunnett's multiple comparisons test for each probe. For **b**, **d**, **f**, **h**, **k**, **p**, **r** and **t**, the mean of the data is presented and error bars indicate s.d.; ns, $P > 0.05$.

https://doi.org/10.1038/s41588-023-01339-5

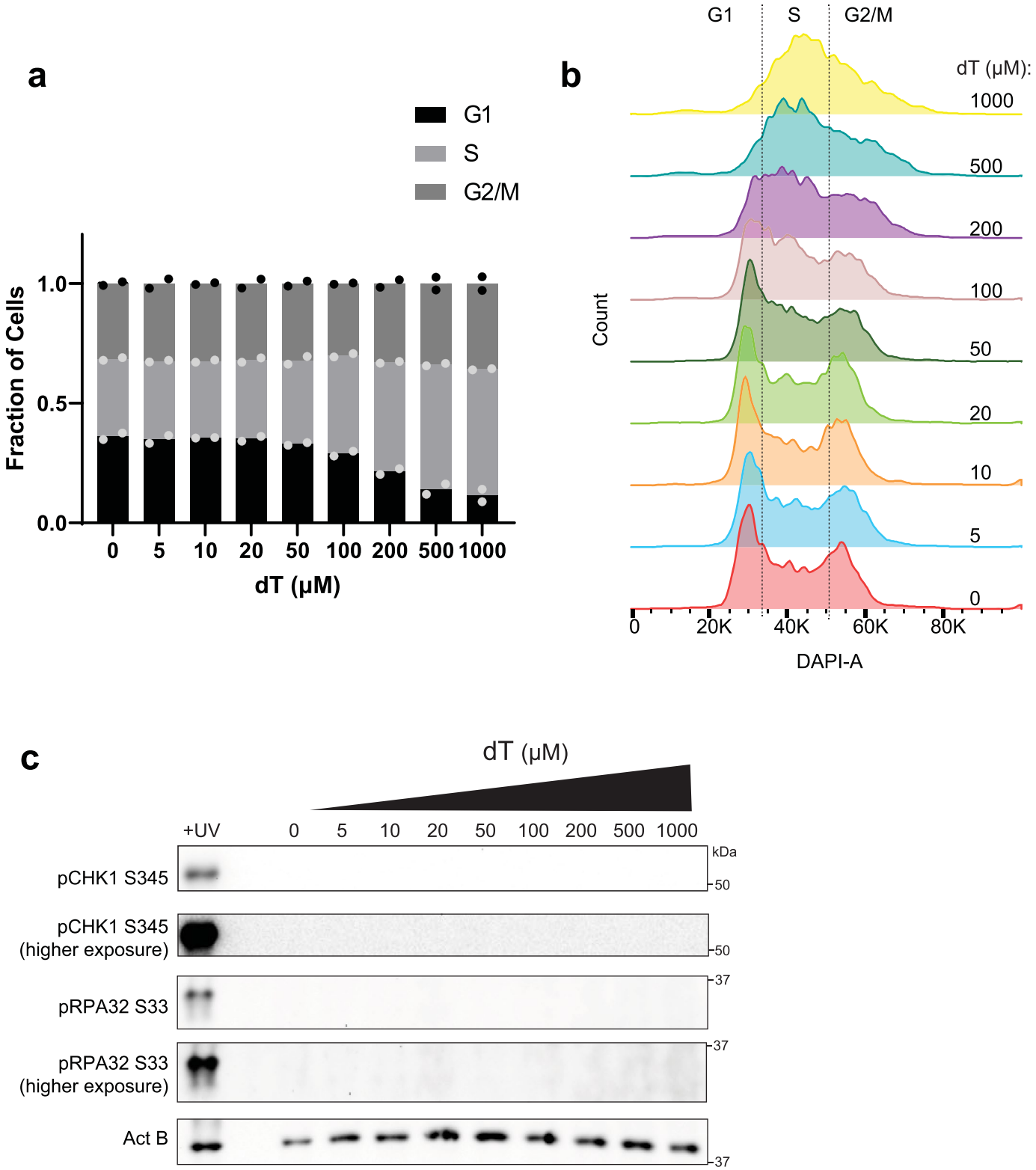

Extended Data Fig. 8 | Effects of dT on iPSC cell cycle progression and replication stress signaling. a, Cell cycle analysis of wild-type iPSCs cultured in the indicated of dose of dT for 24 hours, measured by DAPI staining and flow cytometry, displayed as histograms of DAPI intensity. $n = 2$ biological replicates; the mean of the replicates is presented. **b**, Representative histograms of DAPI signal for cells in **a**. Gates defined based on untreated cells. **c**, Immunoblot of cells treated as in **a**; all images of the same membrane blotted with the indicated primary antibodies. UV- treated cells used as a positive control. Blot shows the results from a single experiment. Full-length blots are provided as source data.

https://doi.org/10.1038/s41588-023-01339-5

a In Homeostasis:

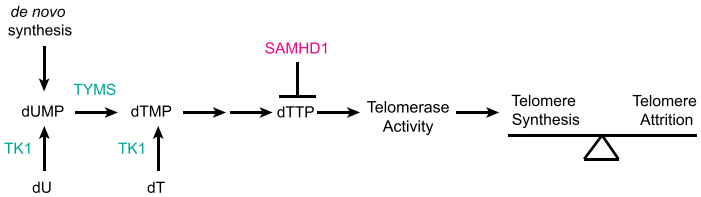

b dT Supplementation:

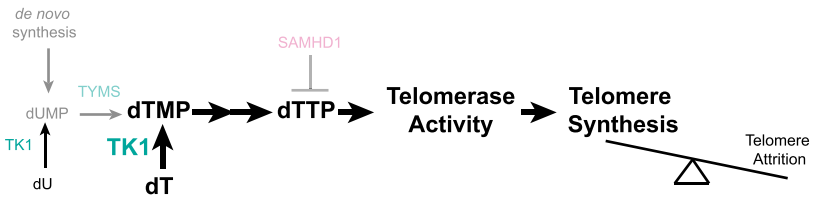

c dU Supplementation:

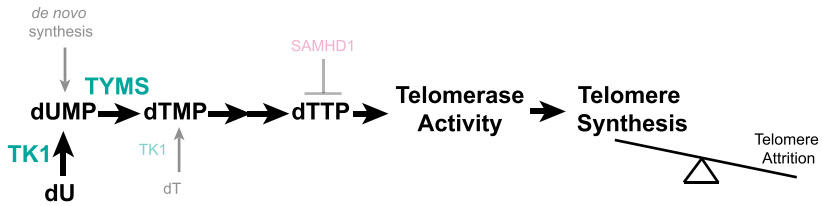

d Loss of SAMHD1:

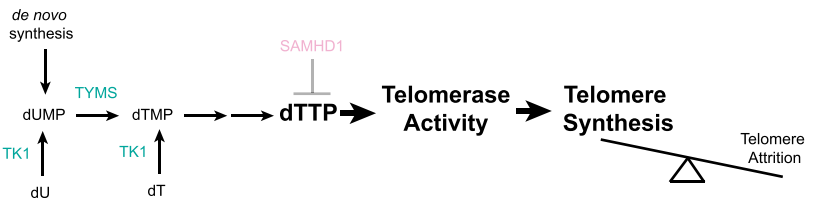

e Treatment with Hydroxyurea or 5FU:

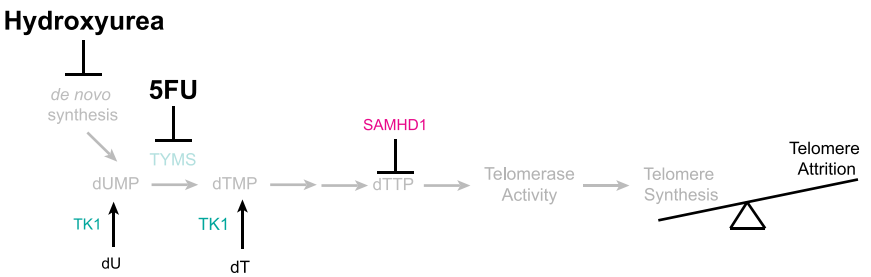

Extended Data Fig. 9 | Model of relationship between dT nucleotide metabolism and telomere synthesis. a-e, Schematics illustrate conditions of homeostasis (**a**), dT supplementation (**b**), dU supplementation (**c**), loss of SAMHD1 (**d**), and treatment with hydroxyurea or 5-fluorouracil (**e**).

nature portfolio

Corresponding author(s): Suneet Agarwal

Last updated by author(s): Feb 8, 2023

Reporting Summary

Nature Portfolio wishes to improve the reproducibility of the work that we publish. This form provides structure for consistency and transparency in reporting. For further information on Nature Portfolio policies, see our Editorial Policies and the Editorial Policy Checklist.

Statistics

For all statistical analyses, confirm that the following items are present in the figure legend, table legend, main text, or Methods section.

n/a	Confirmed
☐	☒ The exact sample size (*n*) for each experimental group/condition, given as a discrete number and unit of measurement
☐	☒ A statement on whether measurements were taken from distinct samples or whether the same sample was measured repeatedly
☐	☒ The statistical test(s) used AND whether they are one- or two-sided *Only common tests should be described solely by name; describe more complex techniques in the Methods section.*
☒	☐ A description of all covariates tested
☐	☒ A description of any assumptions or corrections, such as tests of normality and adjustment for multiple comparisons
☐	☒ A full description of the statistical parameters including central tendency (e.g. means) or other basic estimates (e.g. regression coefficient) AND variation (e.g. standard deviation) or associated estimates of uncertainty (e.g. confidence intervals)
☐	☒ For null hypothesis testing, the test statistic (e.g. *F*, *t*, *r*) with confidence intervals, effect sizes, degrees of freedom and *P* value noted *Give P values as exact values whenever suitable.*
☒	☐ For Bayesian analysis, information on the choice of priors and Markov chain Monte Carlo settings
☒	☐ For hierarchical and complex designs, identification of the appropriate level for tests and full reporting of outcomes
☒	☐ Estimates of effect sizes (e.g. Cohen's *d*, Pearson's *r*), indicating how they were calculated

Our web collection on statistics for biologists contains articles on many of the points above.

Software and code

Policy information about availability of computer code

Data collection	BD FACSDiva 8.0.2, BioRad Image Lab V6.0.
Data analysis	ImageJ V1.53c, Graphpad Prism V9.1.0, FlowJo V10.7.1, MAGeCK Robust Rank Algorithm (RRA) V0.5.9.2, MAGeCKFlute v0.5.9.2, Synthego ICE V3.0, WALTER V2.0., Geneious Prime 2019.2.3, MinKNOW 22.05.5, Bream 7.1.3, Configuration 5.1.5, Guppy 6.1.5, MinKNOW Core 5.1.0, MATLAB R2021a, ggseqlogo V0.1, R V4.1.2. One custom MATLAB script (V1.0) was used to analyze nanopore sequencing data which has been deposited in a public repository and can be accessed at the following link: https://doi.org/10.5281/zenodo.7607615

For manuscripts utilizing custom algorithms or software that are central to the research but not yet described in published literature, software must be made available to editors and reviewers. We strongly encourage code deposition in a community repository (e.g. GitHub). See the Nature Portfolio guidelines for submitting code & software for further information.

Data

Policy information about availability of data

All manuscripts must include a data availability statement. This statement should provide the following information, where applicable:

- Accession codes, unique identifiers, or web links for publicly available datasets
- A description of any restrictions on data availability
- For clinical datasets or third party data, please ensure that the statement adheres to our policy

gRNA library sequencing data and TRAP nanopore sequencing data have been deposited in the Sequence Read Archive, Bio project: PRJNA851386 and are available at https://www.ncbi.nlm.nih.gov/sra/PRJNA851386

Human research participants

Policy information about studies involving human research participants and Sex and Gender in Research.

Reporting on sex and gender	Eight human biospecimens were utilized for the generation of iPSCs, seven of which were from patients with telomere biology disorders. Sex and gender were not considered in study design.
Population characteristics	Human biospecimen donors were of childhood to adult age. Genotypic information of patients diagnosed with dyskeratosis congenita is provided in the figures, and is listed here: wildtype; TERC het. Δ; DKC1 p.A353V; DKC1 p.del37L; PARN p.N7H / Δ; PARN p.S87L / Ø; TINF2 het. p.R282H; DKC1 p.A386T. Age, gender, sex, and treatment characteristics were not considered or relevant for the analyses in this study.
Recruitment	Where appropriate, participants were recruited during clinical encounters in compliance with IRB-approved protocols. Biosamples were de-identified upon acquisition. Because recruitment and collection of deidentified biospecimens occurred prior to the inception of this study, and because the clinical outcome of patients was not relevant, we estimate any potential effects of selection bias to be minimal in regards to the claims made in this study.
Ethics oversight	Boston Children's Hospital Insitutional Review Board

Note that full information on the approval of the study protocol must also be provided in the manuscript.

Field-specific reporting

Please select the one below that is the best fit for your research. If you are not sure, read the appropriate sections before making your selection.

☒ Life sciences ☐ Behavioural & social sciences ☐ Ecological, evolutionary & environmental sciences

For a reference copy of the document with all sections, see nature.com/documents/nr-reporting-summary-flat.pdf

Life sciences study design

All studies must disclose on these points even when the disclosure is negative.

Sample size	No formal sample size calculations were performed. Sample sizes were chosen given our expectation of the variability in the experimental procedures utilized, from prior experience using these methods. As described in the text, biological and technical replicates including the use of multiple cell lines were included throughout the work.
Data exclusions	No data were excluded.
Replication	For our finding that thymidine supplementation increases telomere length, we tested thymidine from different manufacturers, and in multiple independent cell lines / cell types, all with consistent results, with one to twelve biological replicates as described in the figure legends. For studies showing SAMHD1 loss-of-function leads to telomere elongation, we used both shRNA and CRISPR/Cas9 methods and used several cell lines, all with consistent results, with one to three biological replicates as described in the manuscript. Other experiments were performed with biological and technical replicates as described in the figure legends, with consistent results in support of the conclusions drawn.
Randomization	No grouping was necessary for this study because cell lines could be expanded and treated with all experimental arms.
Blinding	Blinding was not performed because it was not required for the objective analyses throughout this study. In order to minimize bias in the interpretation of our findings, standard data analysis tools were used whenever possible to quantify data including gene editing efficiency, gRNA enrichment, and telomere length measurements by Southern blotting.

Reporting for specific materials, systems and methods

We require information from authors about some types of materials, experimental systems and methods used in many studies. Here, indicate whether each material, system or method listed is relevant to your study. If you are not sure if a list item applies to your research, read the appropriate section before selecting a response.

Materials & experimental systems

n/a	Involved in the study
☐	☒ Antibodies
☐	☒ Eukaryotic cell lines
☒	☐ Palaeontology and archaeology
☒	☐ Animals and other organisms
☒	☐ Clinical data
☒	☐ Dual use research of concern

Methods

n/a	Involved in the study
☒	☐ ChIP-seq
☐	☒ Flow cytometry
☒	☐ MRI-based neuroimaging

Antibodies

Antibodies used

Mouse monoclonal anti-SAMHD1 (Origene TA502024, Clone OTI3F5, Lot F001); mouse polyclonal anti-SAMHD1 (Abcam ab67820, lots GR3415677-2 and GR3352313-5), goat polyclonal anti Beta Actin antibody directly conjugated to horseradish peroxidase (Santa Cruz Biotechnology,: sc-1615, C-11, lot G1316); rabbit polyclonal antibody to mouse IgG (H+L) conjugated to horseradish peroxidase (Abcam, ab6728, Lot GR3383345-3); rabbit monoclonal anti pCHK1-S345 (Cell Signaling Technologies, clone 133D3, 2348S, lot 18); rabbit polyclonal anti pRPA32-S33 (Bethyl Laboratories A300-246A, lot 11); goat polyclonal antibody to rabbit IgG (H+L) conjugated to horseradish peroxidase (BioRad 1705046 lot 64340912); mouse IgG1 monoclonal antibody against the HA tag conjugated to magnetic beads (Sigma-Aldrich, SAE0197, Clone HA-7, Lot 0000185652).

Validation

Primary antibodies were validated as follows: SAMHD1 antibodies were validated using knockdown, knockout, or overexpression as demonstrated in Extended Data Figure 4. The Abcam SAMHD1 antibody was further validated by its manufacturer via overexpression (see https://www.abcam.com/samhd1-antibody-ab67820.html). The Origene SAMHD1 antibody was also validated by its manufacturer using gene knockout and overexpression (see https://www.origene.com/catalog/antibodies/primary-antibodies/ta502024/samhd1-mouse-monoclonal-antibody-clone-id-oti3f5). The beta actin antibody was validated by its manufacturers using western blot and immunofluorescence (see https://datasheets.scbt.com/sc-1615.pdf). Anti pCHK1-S345 and Anti pRPA32-S33 antibodies were validated by showing specific signal at the expected molecular weight in UV irradiated cells as shown in Figure 6 and Extended Data Figure 8. The anti-pCHK1-S345 antibody was also validated by its manufacturer using UV-treatment (see https://www.cellsignal.com/products/primary-antibodies/phospho-chk1-ser345-133d3-rabbit-mab/2348). The Anti pRPA32-S33 was also validated by its manufacturer using etoposide treatment (see https://www.thermofisher.com/antibody/product/Phospho-RPA32-Ser33-Antibody-Polyclonal/A300-246A). Anti-HA conjugated magnetic beads immunoprecipitated active HA-tagged telomerase enzyme compared to control as shown in Figure 7. The anti HA antibody clone was also validated by its manufacturer using overexpression (see https://www.sigmaaldrich.com/US/en/product/sigma/h9658).

Eukaryotic cell lines

Policy information about cell lines and Sex and Gender in Research

Cell line source(s)

K562 (ATCC), HEK293T (ATCC), patient derived iPSCs lines were generated at Boston Children's Hospital using standard procedures.

Authentication

iPSC lines were genotyped to verify they harbor the indicated disease causing mutation. K562 and HEK293T cell lines were not authenticated.

Mycoplasma contamination

All cells tested negative for mycoplasma contamination by PCR.

Commonly misidentified lines
(See ICLAC register)

No commonly misidentified cell lines were used in this study.

Flow Cytometry

Plots

Confirm that:

☒ The axis labels state the marker and fluorochrome used (e.g. CD4-FITC).

☒ The axis scales are clearly visible. Include numbers along axes only for bottom left plot of group (a 'group' is an analysis of identical markers).

☐ All plots are contour plots with outliers or pseudocolor plots.

☒ A numerical value for number of cells or percentage (with statistics) is provided.

Methodology

Sample preparation	Flow-FISH was performed on HEK293T or K562 cells as follows. Cells were washed with 4.5% dextrose, 10mM HEPES, .1% BSA, then resuspended in 80% formamide, 20mM NaCl, 20mM TrisHCl, 1% BSA with 1ug/mL AlexaFluor-647 conjugated TelC PNA probe, heated to 82C for 20 minutes, then incubated at room temperature for 2 hours followed by four washes with 75% formamide, 20mM TrisHCl, .1% BSA, .1% Tween 20, then washed once with 4.5% dextrose, 10mM HEPES, .1% BSA .1% tween 20, followed by resuspension in PBS with .1% Triton-X and DAPI. For DAPI staining presented in Figure 6, Extended Data Figure 6, and Extended Data Figure 8, cells were harvested, resuspended in 50ul PBS 2% FBS, then 1ml of cold 70% ethanol was added followed by fixation at -20C for at least 2 hours. Cells were then washed in 500ul 2% FBS PBS, incubated for 15 minutes, then resuspended in PBS with 0.1% Triton-X and DAPI.
Instrument	Cells were sorted using either a BD FACSARIA II or FACSARIA III at the Boston Children's Hospital flow cytometry core. Analysis was performed on a BD LSR-II or BD Fortessa at the Boston Children's Hospital flow cytometry core.
Software	Data was collected using the BD FACSDiva 8.0.2 software and analyzed using FlowJo V10.7.1.
Cell population abundance	Cells meeting the described gates were sorted based on TelC-A647 as described in the text. Enrichment of gRNAs targeting known telomere length regulating genes indicates sorted populations were comprised of cells with long or short telomere length. Counts for sorted populations: Genome-wide screen (in millions of cells) sorted low A647 replicate 1: 1.27, replicate 2 1.89; sorted high A647 replicate 1: 1.05, replicate 2: 1.14. Nucleotide metabolism targeted screen (in thousands of cells): sorted low A647 replicate 1: 164, replicate 2: 82; sorted high A647 replicate 1: 232, replicate 2: 108.
Gating strategy	Typical gating strategies involved gating on FSC/SSC properties, exclusion of cell doublets, gating on DAPI low cells to only sort cells with 2N genomes, then sorting the cells with the highest and lowest AlexaFluor647 signal based on the percentiles described in the text.

☒ Tick this box to confirm that a figure exemplifying the gating strategy is provided in the Supplementary Information.